LRP1 controls biosynthetic and endocytic trafficking of neuronal prion protein

Celia J. Parkyn[1], Esmeralda G. M. Vermeulen[1], Roy C. Mootoosamy[1], Claire Sunyach[1,*], Christian Jacobsen[2], Claus Oxvig[2], Søren Moestrup[2], Qiang Liu[3], Guojun Bu[3], Angela Jen[1] and Roger J. Morris[1,‡]

[1]King's College London, Wolfson Centre for Age Related Disease, Guy's Campus, London SE1 1UL, UK
[2]Department of Medical Biochemistry, University of Aarhus, DK-8000 Aarhus C, Denmark
[3]Department of Pediatrics, Washington University School of Medicine, St Louis Children's Hospital, St Louis MO 63110, USA
*Present address: IPMC du CNRS, UPR411, 660 Route del Lucioles, 06560 Valbonne, France
‡Author for correspondence (e-mail: roger.morris@kcl.ac.uk)

Accepted 19 December 2007
Journal of Cell Science 121, 773-783 Published by The Company of Biologists 2008
doi:10.1242/jcs.021816

Summary

The trafficking of normal cellular prion protein (PrP^C) is believed to control its conversion to the altered conformation (designated PrP^{Sc}) associated with prion disease. Although anchored to the membrane by means of glycosylphosphatidylinositol (GPI), PrP^C on neurons is rapidly and constitutively endocytosed by means of coated pits, a property dependent upon basic amino acids at its N-terminus. Here, we show that low-density lipoprotein receptor-related protein 1 (LRP1), which binds to multiple ligands through basic motifs, associates with PrP^C during its endocytosis and is functionally required for this process. Moreover, sustained inhibition of LRP1 levels by siRNA leads to the accumulation of PrP^C in biosynthetic compartments, with a concomitant lowering of surface PrP^C, suggesting that LRP1 expedites the trafficking of PrP^C to the neuronal surface. PrP^C and LRP1 can be co-immunoprecipitated from the endoplasmic reticulum in normal neurons. The N-terminal domain of PrP^C binds to purified human LRP1 with nanomolar affinity, even in the presence of 1 μM of the LRP-specific chaperone, receptor-associated protein (RAP). Taken together, these data argue that LRP1 controls both the surface, and biosynthetic, trafficking of PrP^C in neurons.

Supplementary material available online at
http://jcs.biologists.org/cgi/content/full/121/6/773/DC1

Key words: Biosynthesis, Endocytosis, Endoplasmic reticulum, Golgi, LRP, Prion protein

Introduction

PrP^C is endocytosed by mechanisms that differ according to the cell type studied, presumably reflecting differences in the expression of partner proteins that determine the trafficking of PrP^C that lacks a cytoplasmic domain into which endocytic trafficking motifs could be embedded. On N2a cells, PrP^C is endocytosed constitutively by means of coated pits (Shyng et al., 1994; Sunyach et al., 2003); whereas cells that do not endogenously express PrP^C but transfected with a vector encoding PrP^C can require 100 μM Cu^{2+} to initiate coated pit endocytosis (Taylor and Hooper, 2007) or else slowly internalise PrP^C by non-coated pit mechanisms (Peters et al., 2003).

The cell type of prime relevance to mammalian prion biology is the neuron. PrP^C occupies lipid rafts that, on neurons, are distinctive, differing both chemically and spatially from those containing the major neuronal glycosylphosphatidylinositol (GPI)-anchored protein, Thy-1 (Brügger et al., 2004; Madore et al., 1999; Sunyach et al., 2003). PrP^C exits its rafts to traverse detergent-soluble membrane as it enters coated pits for endocytosis and then recycles back to the surface via perinuclear sorting compartments, the entire cycle taking 6-10 minutes (Morris et al., 2006; Sunyach et al., 2003).

PrP^C has two distinct domains (Fig. 1): a GPI-anchored, α-helical C-terminal domain (amino acids 126-231) and an unstructured N-terminal domain (residues 23-125) that is necessary and sufficient for coated pit endocytosis (Shyng et al., 1995a; Sunyach et al., 2003), with the immediate N-terminal basic motif (NH_2-KKRPKP-) being essential for this process (Sunyach et al., 2003).

Binding through a basic motif to low-density lipoprotein receptor-related protein 1 (LRP1) is the mechanism by which the GPI-anchored urokinase plasminogen activator receptor is internalised by means of coated pits (Horn et al., 1998). This prompted us to investigate whether LRP1 is the endocytic partner for neuronal PrP^C (Morris et al., 2006). Recently, Taylor and Hooper (Taylor and Hooper, 2007) reported that LRP1 is required for the Cu^{2+}-dependent endocytosis of exogenous PrP^C on SH-SY5Y cells.

LRP1 is a massive protein (~600 kDa) that is proteolytically nicked during biosynthesis to give two stably associated polypeptides: an 85-kDa membrane-spanning C-terminal fragment and a 515-kDa extracellular N-terminal chain (Fig. 1). LRP1 is expressed abundantly on neurons (Bu et al., 1994; Moestrup et al., 1992), where its fundamental role is the uptake of cholesterol and fatty acids by these cells whose vast membrane processes require the import of glial-derived sterol and lipid for growth and synapse formation (Mauch et al., 2001). In addition, LRP1 binds to >30 ligands extracellularly, and its cytoplasmic domain binds to endocytic and scaffold adaptors that link the receptor to other membrane proteins, including Alzheimer's precursor protein (APP) (Herz and Chen, 2006; Zerbinatti et al., 2004). The LRP1 knockout mouse is embryonic lethal, and even a partial knockout in adult brain results in slow lethality (May et al., 2004).

LRP family members have a specific chaperone, receptor-associated protein (RAP), that masks their ligand-binding sites during biosynthesis. Recombinant RAP added externally to cells

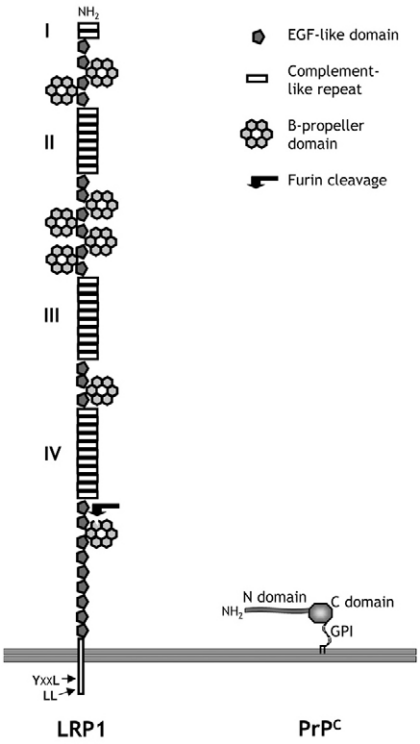

Fig. 1. Schematic view of the domain structure of LRP1 [adapted from Li et al. (Li et al., 2000) and Springer (Springer, 1998)] and PrP^C, for which the flexible N- and structured C-terminal domains, and GPI anchor, are indicated; grey lines represent the surface membrane. LRP1 domains and the site of furin cleavage are indicated; Roman numerals indicate the four repeats of the ligand-binding complement-like domains; endocytic motifs are indicated in the cytoplasmic domain. LRP1, with >4500 amino acids, is more than 20 times larger than PrP^C (208 amino acids).

inhibits the binding and endocytosis of LRP ligands (Iadonato et al., 1993; Moestrup et al., 1993b).

PrP^C has also been ascribed numerous binding partners (Linden et al., 2007). Any attempt to add to its list of molecular associates needs to demonstrate both specificity and biological relevance. One reported receptor for PrP is the laminin precursor protein (confusingly also abbreviated 'LRP') (Gauczynski et al., 2001) that functions both as a cytoplasmic ribosomal subunit and a broad-specificity adhesive protein on the cell surface (Kazmin et al., 2003).

We report here that LRP1 associates with endogenously expressed PrP^C on the neuronal cell surface to internalise it and, furthermore, that LRP1 binds to PrP^C in biosynthetic compartments to assist its trafficking to the neuronal surface.

Results

Colocalisation of LRP1 and PrP^C on the cell surface

Sensory neurons are in this study used because in vivo they uniquely have axons and no dendrites; thus, lacking any synaptic input, they are not denervated upon being dissociated and so survive, remain differentiated and regenerate their axons when introduced into culture from adult tissue (Scott, 1977). In dissociated culture, they extend axons over laminin-coated substrates and flattened satellite cells, while their large cell bodies float, usually without contacting other cells, into the medium above. Fig. 2A,B shows immunolabelling for PrP^C at the level of the substrate, and the zone 6 μm above this, where the large neuronal cell bodies are suitable

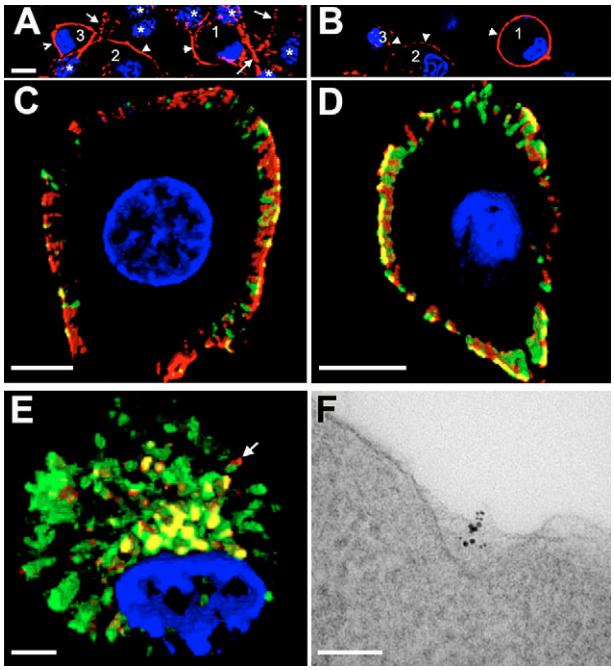

Fig. 2. Immunohistochemical localisation of PrP^C and LRP1 on sensory neurons. (A,B) Immunolabelling for cell-surface PrP^C with 2S Alexa-Fluor-594–Fab (red), 3 μm (A) and 9 μm (B) above the plane of the laminin substrate. PrP^C-expressing neurons (1-3; arrowheads point to their surface labelling), plus axons (arrows), and PrP^C-negative substrate cells (visible by their blue DAPI-stained chromatin, asterisks) can be seen in (A); only their cell bodies are visible in B. These images are from a series (supplementary material Fig. S1), collected every 100 nm in vertical steps, which were deconvolved and assembled into ascending stacks of ten sections (i.e. 1 μm optical sections). Neuronal cell bodies shown subsequently in this paper are combined from stacks of 10-30 images taken at a level corresponding to B, with DAPI-stained chromatin. (C,D) Surface immunolabelling of PrP^C (2S Alexa-Fluor-594–Fab, red) and green Alexa-Fluor-488-labelled anti-LRP1 (C) or Ctx (D) on sensory neurons fixed at 37°C before immunolabelling. On the cells shown, 37% and 77% of PrP colocalised with LRP1 and Ctx (data are in supplementary material Tables S1a and S1b). (E) Neuron with surface PrP^C prelabelled at 10°C with Alexa-Fluor-594–Fab (red), then allowed to endocytose at 37°C for 1 minute, then fixed, permeabilised and immunolabelled for LRP1. It had endocytosed 82% of its labelled PrP^C, most to perinuclear tubular structures (yellow owing to colocalised LRP1); arrow points to labelled PrP^C still on the surface. (F) Transmission EM showing labelling within a coated pit on a neuron that has endocytosed (1.5 minutes at 37°C) its prelabelled 5 nm gold-Fab to PrP^C, and 10 nm gold-α_2M*. Bars, 5 μm (A,C-E), 100 nm (F).

for analysis of the endocytic trafficking of fluorescently labelled surface proteins.

Fig. 2C is an immunofluorescent view of the relative distribution of LRP1 and PrP^C on the surface of a cultured adult sensory neuron. Partial colocalisation of the two proteins was found, with 40% of PrP^C overlapping LRP1 (Table 1; conversely, 43.2±14.7% of surface LRP1 colocalised with PrP^C). Somewhat higher colocalisation (54.2±21.6%) was seen between PrP^C and the lipid 'raft' marker ganglioside GM1 labelled with the cholera toxin B chain (Ctx; Fig. 2D). Antibodies against other neuronally expressed LRP family members (LRP1b, LRP6, LRP8 and VLDLR) failed to react with sensory neurons assessed by immunoblotting or immunohistochemistry.

To gain a more dynamic view of the proximity of the two proteins during endocytosis, surface PrP^C was prelabelled at 10°C with monovalent 2S Alexa-Fluor-594–Fab to PrP^C; the cells were then

Table 1. Immunofluorescent colocalisation with LRP1 of PrP^C, prelabelled with Alexa-Fluor-594 Fab, remaining on the surface during endocytosis

Time at 37°C	% PrP colocalised with LRP1†	% Fab-labelled PrP^C still on surface
0 minutes	40.6±18.9, *n*=8	82.4±14.4
1 minutes	60.1±13.9*, *n*=9	49.2±20.0
2 minutes	97.7±2.9**, *n*=14	13.3±6.9

†Mean percentage (± s.d.); *P<0.05 and **P<0.001, significantly different from 0-minute value. For experimental data, see supplementary material Table S1a.

washed to remove unbound Fab and placed at 37°C. The pulse-labelled PrP^C was endocytosed rapidly over the next 2 minutes (Fig. 2E), a period during which labelled PrP^C remaining on the cell surface colocalised increasingly with LRP1 (Table 1).

The proximity of PrP^C to LRP1 during endocytosis was analysed at higher resolution by examining, by transmission electron microscopy (EM), neurons that were prelabelled for PrP^C with 5 nm Fab gold, and for LRP1 by its ligand, activated $\alpha_2$macroglobulin (α_2M*), attached to 10 nm gold. Also, for comparison with PrP^C, the transferrin (Tf) receptor was labelled with Tf coupled to 10 nm gold. After endocytosis for 1.5 minutes at 37°C, within the restricted confines of coated pits, 66.2% of PrP^C label was within 50 nm of α_2M* (Fig. 2F), but only 24.3% was within 50 nm of the Tf label. The converse selective association of the ligands with PrP^C also held: 84.7% of α_2M* was within 50 nm of PrP^C, compared with only 35.4% of Tf. Thus, within this morphologically identifiable endocytic compartment, PrP^C was more closely associated with an LRP1 ligand than with a ligand for an independently endocytosed receptor.

Inhibition of the endocytosis of PrP^C by recombinant RAP and $siRNA^{LRP1}$

To assess inhibition of endocytosis, neurons were prelabelled for surface PrP^C with 2S Alexa 594-Fab; as a positive control, their Tf receptors were labelled with Alexa-Fluor-488–Tf. Preincubation with recombinant RAP inhibited endocytosis of PrP^C but not Tf (Fig. 3A,B; Table 2).

To circumvent long-term disruption of neuronal metabolism by stable inhibition of LRP1 expression, transient knockdown of LRP1 was achieved using the antennapedia peptide penetratin-1 to deliver one of three siRNAs specific for LRP1 ($siRNA^{LRP1.1}$, $siRNA^{LRP1.2}$, $siRNA^{LRP1.3}$) or a control ($siRNA^{Con}$). The $siRNA^{LRP1.1}$ produced

Table 2. Inhibition of endocytosis of PrP^C and Tf by RAP and $siRNA^{LRP1}$†

Inhibiting agent	% PrP^C internalised	% Tf internalised
Vehicle control	93.2±1.6	93.0±2.3
+80 nM RAP	64.5±4.1**	88.2±7.2
+1 μM RAP	29.1±5.0**	94.5±0.5
$siRNA^{Con}$	84.9±15.0	87.5±10.9
$siRNA^{LRP1.1}$	47.1±14.2**	80.5±13.4
$siRNA^{LRP1.2}$	63.0±26.3**	85.2±7.1
$siRNA^{LRP1.3}$	68.5±16.2*	82.7±11.9

†Mean ± s.d. of surface-labelled PrP^C or Tf internalised in 2 minutes at 37°C; significant differences from control values, *P<0.01 and **P<0.001. For experimental data, see supplementary material Tables S2a, S2b, S2c and S2d.

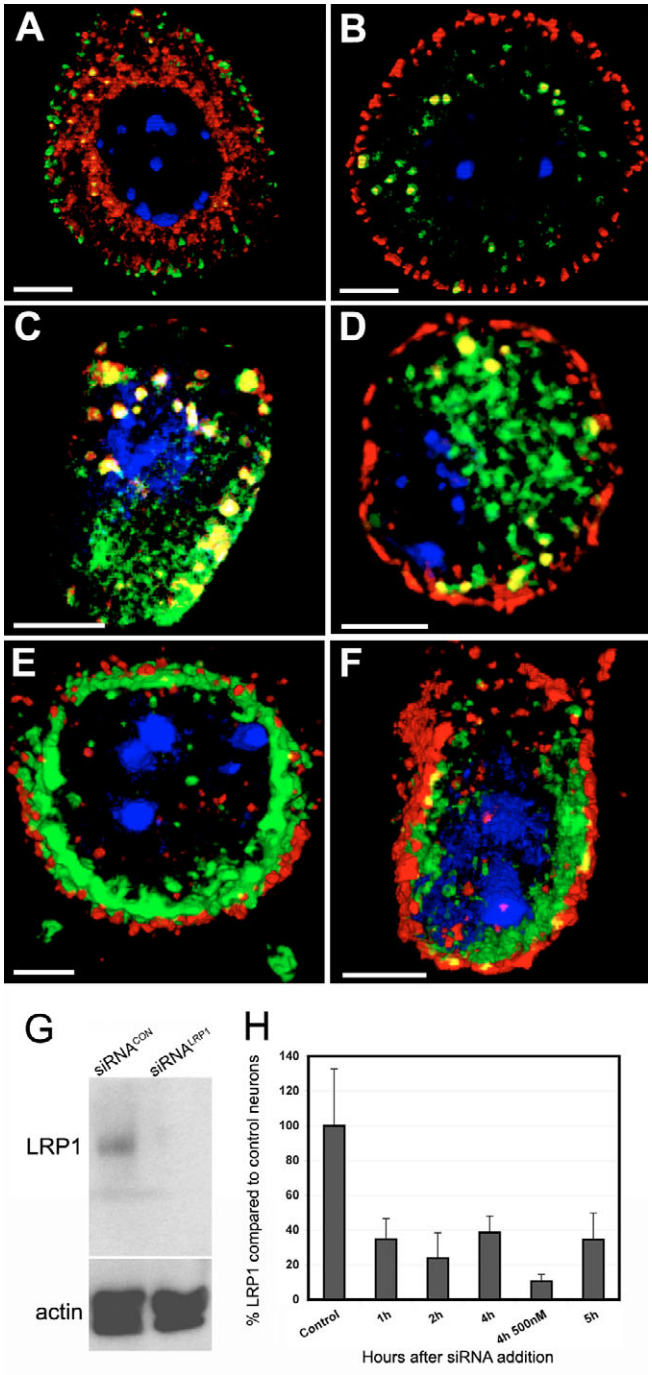

Fig. 3. Inhibition of endocytosis of PrP^C on sensory neurons by RAP and $siRNA^{LRP1}$. (A,B) 1 μM RAP (B; A is vehicle control) inhibits the endocytosis of neuronal surface-labelled PrP^C (red) but not Tf (green) after 2 minutes at 37°C. (C,D) Neurons treated for 90 minutes with 250 nM $siRNA^{Con}$ (C) or $siRNA^{LRP1.1}$ (D) before endocytosing surface-labelled PrP^C (red) and Tf (green) for 2 minutes at 37°C. (E,F) Immunocytochemical labelling of surface PrP^C (red) and total LRP1 (green) in neurons preincubated for 90 minutes with 250 nM $siRNA^{Con}$ (E) or $siRNA^{LRP1}$ (F), used to assess the effect of LRP1 knockdown; data in supplementary material Tables S2c and S2d. Bars, 5 μm. (G,H) Reduction of LRP1 protein shown by immunoblot (G; the 515-kDa band is shown) and quantitated in H (mean band intensity normalised to actin, ±s.d., *n*=4 independent knockdown experiments) after 250 nM penetratin-siRNA addition for the times shown (plus a 4-hour point showing the effect of adding additional 250 nM siRNA at 2 hours). The samples shown in G were from the 4-hour time point with two additions of siRNA.

rapid knockdown of LRP1 protein (Fig. 3E-H) that was followed by several-fold overexpression by 72 hours (data not shown). For inhibition of endocytosis, 90 minutes of treatment of sensory neurons with the siRNA-penetratin conjugate was used, as each of the three siRNAs directed against LRP1 lowered expression of LRP1 protein by 30-50% within this period without affecting the level of surface PrP^C, as determined by quantitative analysis of immunofluorescent binding to surface PrP^C and total cellular LRP1 (Fig. 3E,F). For example, in an experiment in which $siRNA^{LRP1.1}$ lowered expression of LRP1 to 64.0% of the control level (P=0.003), the level of surface PrP^C on the two sets of cells was identical (P=0.98; supplementary material Table S2c). With this brief downregulation of LRP1, all three $siRNA^{LRP1}$ constructs significantly inhibited the endocytosis of PrP^C but not Tf (Table 2; Fig. 3C,D).

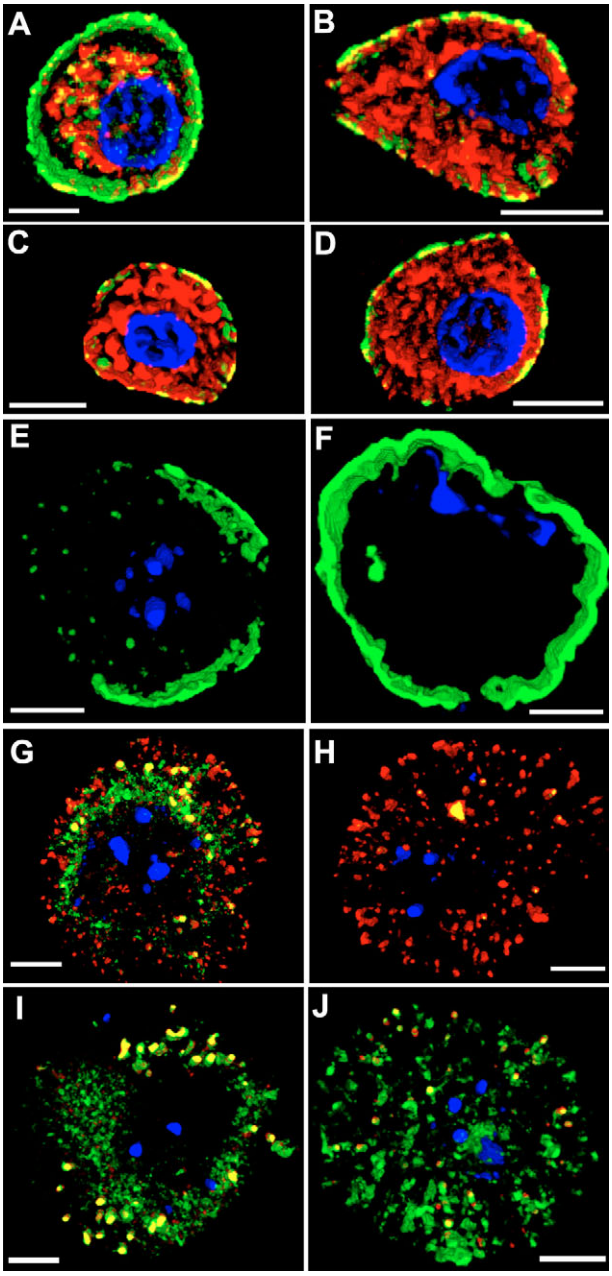

Fig. 4. Effect of 4 hours of treatment with $siRNA^{LRP1}$ upon PrP^C distribution within neurons, and upon LRP1-dependent endocytosis. (A-D) Neurons pretreated with 250 nM $siRNA^{Con}$ (A), or with $siRNA^{LRP1.1}$ (B), $siRNA^{LRP1.2}$ (C) or $siRNA^{LRP1.3}$ (D), were surface labelled with Alexa-Fluor-488–2S Fab anti-PrP (green), then fixed and permeabilised for labelling internal PrP^C with Alexa-Fluor-594–SAF83 (red). Quantitation is given in supplementary material Table S4a. (E,F) Neurons treated as above with $siRNA^{Con}$ (E) or $siRNA^{LRP1.1}$ (F), fixed, permeabilised and labelled (both surface and internal) with Alexa-Fluor-488 anti-Thy-1 antibody (green). Quantitation is given in supplementary material Table S3b. (G,H) Neurons treated with $siRNA^{Con}$ (G) or $siRNA^{LRP1.1}$ (H) were prelabelled with Alexa-Fluor-488α_2M* (green) and Texas Red-Tf and then placed at 37°C for 2 minutes. (I,J) Neurons treated with $siRNA^{Con}$ (I) or $siRNA^{LRP1.1}$ (J) were prelabelled for PrP^C with Alexa-Fluor-594–Fab (red), and the transferrin receptor with Alexa-Fluor-488–Tf (green), and placed at 37˚C for 2 minutes. Bars, 5 μm.

Sustained inhibition of LRP1 lowers the level, but not endocytosis, of surface PrP^C

Exposure of neurons to $siRNA^{LRP1.1}$ for 2-4 hours reduced LRP1 levels by ~75% (Fig. 3G,H). This was accompanied by a marked reduction in surface PrP^C, to 43.9±8.1% of $siRNA^{Con}$-treated cells within 4 hours, as determined by immunolabelling of live cells at 10°C (Fig. 4A-D; P<0.001; supplementary material Table S3a). This treatment increased the surface level of GPI-anchored Thy-1 (Fig. 4E,F) by 2.2±1.2 fold compared with controls (P=0.04; supplementary material Table S3b). The increased Thy-1 was evident in immunoblots, as was an even larger increase in APP (Fig. 5).

Sustained reduction of LRP1 levels did not affect the ability of the residual surface LRP1 to be endocytosed, as shown by the complete internalisation within 2 minutes of much reduced levels of its ligand, α_2M* (Fig. 4G,H). Similarly, the reduced level of surface PrP^C was >80% endocytosed within 2 minutes (Fig. 4I,J), giving a reduced amount of PrP^C endocytosed without any discernible reduction in its rate of endocytosis.

Sustained inhibition of LRP1 increases PrP^C in biosynthetic compartments

However, $siRNA^{LRP1}$ inhibition for 4 hours was accompanied not only by a loss in surface PrP^C but also by a 3.5±0.9 (P<0.01) fold increase in intracellular PrP^C (Fig. 4A-D). Intracellular Thy-1 was not elevated (Fig. 4E,F).

Most of the increased intracellular PrP^C colocalised with early biosynthetic compartments (Table 3; Fig. 6). The chaperone BiP was used as a marker of the endoplasmic reticulum (ER); α-

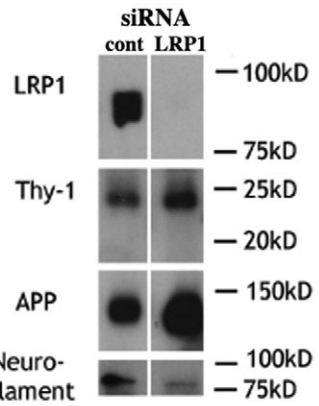

Fig. 5. Effect of prolonged downregulation of LRP1 on the neuronal proteins Thy-1 and APP. Immunoblots, with the neurofilament light chain used as a loading control, of cells treated for 5 hours with two additions of 250 nM siRNA, control (left) and LRP1.1 (right).

Table 3. Effect of decreasing LRP1 with respect to PrP^C upon the colocalisation of PrP^C with markers of biosynthetic compartments in sensory neurons†

Neurons (modification)	Modifier	% BiP (ER)	% α-Mannosidase II (mid-Golgi)	% Syntaxin 6 (trans-Golgi)
WT (control)	$siRNA^{Con}$	54.6±22.1	22.1±9.5	25.5±17.7
WT (LRP1 lowered)	$siRNA^{LRP1.1}$	29.9±18.3*	23.3±7.0	18.3±10.7
Tg20 (PrP^C raised)	Transgenic overexpression	27.4±5.8*	25.2±8.9	20.3±4.4

†For experimental data, see supplementary material Tables S4a and S4b. *P<0.05, significant differences from control values.

mannosidase II as a marker for the mid-Golgi, and syntaxin 6 as a marker for the trans-Golgi. The levels of the latter two did not differ between $siRNA^{Con}$ and $siRNA^{LRP1.1}$-treated cells (P>0.5), but BiP levels were elevated 4.4±0.9 fold (P<0.05), suggesting that an ER stress response had been induced. However, the proportion of intracellular PrP^C that colocalised with BiP was nearly halved in the $siRNA^{LRP1.1}$-treated cells (Table 3), so this compartment contained 1.9 fold the normal PrP^C level. The mid- and trans-Golgi retained their normal share of intracellular PrP^C (and so contained 3.5 times their normal PrP^C).

Increased intracellular PrP^C is not induced by ER stress

To test whether the accumulation of PrP^C along biosynthetic pathways is due to an ER stress response, neurons were heat-shocked at 39°C for 4 hours. BiP levels were elevated 2.5 fold compared with their basal levels at 37°C (P=0.015). There was a minor, insignificant decrease in both surface and intracellular PrP^C levels (supplementary material Fig. S2 and supplementary material Tables S5a and S5b).

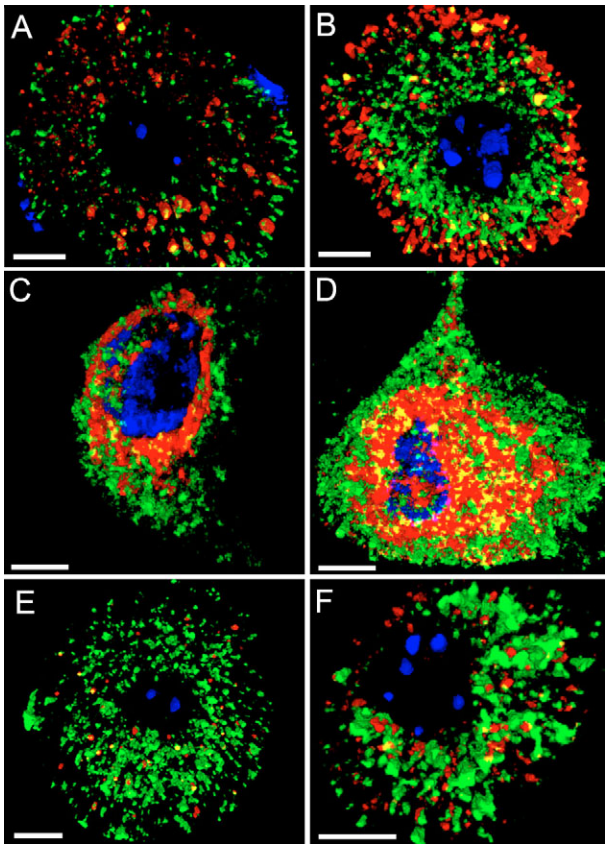

Fig. 6. Effect of lowering LRP1 levels upon internal PrP^C in sensory neurons. (A-F) Neurons treated for 4 hours with 250 nM $siRNA^{Con}$ (A,C,E) or $siRNA^{LRP1.1}$ (B,D,F) were fixed, permeabilised and immunolabelled for PrP^C (green) and (in red) BiP (A,B), α-mannosidase II (C,D) or syntaxin 6 (E,F). Bars, 5 μm.

Increased PrP^C expression mirrors decreased LRP1 expression in its effects upon PrP^C trafficking

Transgenic overexpression of PrP^C, in lowering the ratio of LRP1:PrP^C, should affect PrP^C trafficking in the same way as downregulation of LRP1 if the latter is an obligate trafficking partner. Sensory neurons from PrP^C-overexpressing Tg20 mice were found to have 14-fold higher PrP^C levels than genetically wild-type (WT) neurons (similar to the increased expression reported in brain) (Fischer et al., 1996) and a much smaller (1.8 fold) elevation in their LRP1 level. As a result, Tg20 neurons have an eightfold higher than normal ratio of PrP^C to LRP1 (supplementary material Table S6a).

The excess PrP^C was evident in the time taken by Tg20 sensory neurons to endocytose their surface-labelled PrP^C. WT neurons internalised >80% of surface-labelled PrP^C within 2 minutes at 37°C, irrespective of the level of surface PrP^C they expressed (which varied over a tenfold range; Fig. 7A, left panel). Tg20 PrP^C-overexpressing neurons internalised only a small proportion of their surface-labelled PrP^C at this stage, with a strong inverse correlation between the level of PrP^C expressed and the proportion endocytosed (Fig. 7A, right panel). Even after 6 minutes at 37°C, the highest PrP^C-expressing Tg20 neurons still had ~40% left on their surface (Fig. 7A,B; Table 4). This endocytosis of PrP^C was strongly inhibited by $siRNA^{LRP1.1}$ (Fig. 7B,C; Table 4). Thus, at high levels of overexpression of PrP^C, the expression level of LRP1 becomes rate limiting for PrP^C.

Transgenic overexpression of PrP^C also selectively increased intracellular PrP^C, evident by comparing the ratio of the intensity of immunofluorescent labelling of internal to surface PrP^C in optical cross-sections of neurons (Fig. 7D,E). This ratio was 1.4±1.3 for WT cells, compared with 5.0±1.5 for Tg20 neurons (Table 5), indicating a selective intracellular accumulation of PrP^C at the expense of surface levels in the overexpressing neurons. This mirrors the accumulation of intracellular PrP^C in biosynthetic compartments

Table 4. Proportion of surface-labelled PrP^C and Tf internalised after 6 minutes at 37°C by normal (WT) and transgenic overexpressing (Tg20) neurons†

	$siRNA^{Con}$		$siRNA^{LRP1.1}$	
	% PrP^C	% Tf	% PrP^C	% Tf
WT	83.7±17.5	92.4±5.3	35.8±18.5**	83.4±11.4
Tg 20	58.5±35.3	88.1±8.7	37.4±23.8*	69.3±20.8

†Mean ± s.d. shown. *P<0.1 and **P<0.001, significantly different from the $siRNA^{Con}$ values.

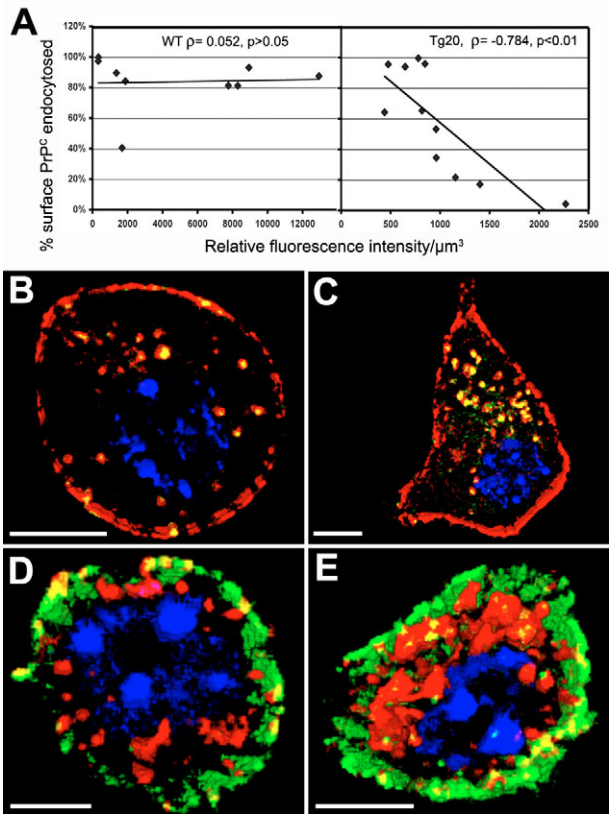

Fig. 7. Effect of overexpression of PrP^C upon its endocytic and biosynthetic trafficking. (A) The percentage of surface-labelled PrP^C on WT (left panel) and Tg20 neurons (right panel) that has been endocytosed is plotted as a function of their relative level of surface PrP^C (measured as the fluorescence intensity of Alexa-Fluor-594–2S Fab bound per μm^3). The correlation coefficient ρ and its significance (p) are shown. To avoid saturation of the camera by the 14-fold brighter fluorescence of Tg20 neurons, excitation intensity was turned down to give an overall fluorescence measured that was approximately comparable for the two sets of neurons. (B,C) tg20 neurons, treated for 90 minutes with $siRNA^{Con}$ (B) or $siRNA^{LRP1.1}$ (C), labelled with 2S Alexa-Fluor-594–Fab (red) and Alexa-Fluor-488–Tf (green) were placed at 37°C for 6 minutes. In the control cell shown, 50% of the labelled PrP^C has been internalised, and 35% in the $siRNA^{LRP1.1}$-treated cell. (D,E) Examples of immunolabelling of WT (D) and Tg20 (E) neurons for cell-surface PrP (Alexa-Fluor-488–2S fab; green) and internal PrP^C (Alexa-Fluor-594–SAF83, red). Bars, 5 μm.

Table 5. Ratio of internal PrP to surface PrP for WT and Tg20 neurons†

Cell no.	WT	Tg20
1	1.17	5.37
2	2.61	5.24
3	0.69	3.73
4	3.20	4.15
5	1.26	3.01
6	0.35	5.54
7	0.17	4.89
8		7.90
Average	1.4	5.0
± s.d.	1.3	1.5
t test, *P*=	0.0001	

†The ratio of internal PrP^C to surface PrP^C is shown for individual cells, determined by differential immunolabelling of surface and internal PrP^C, as shown in Fig. 4A-D.

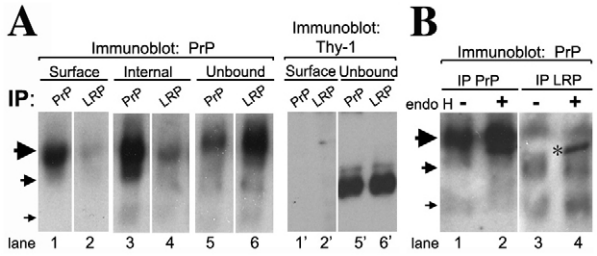

Fig. 8. Biochemical analysis of interaction between PrP^C and LRP1 on sensory neurons. (A) Immunoblot for PrP and Thy-1 of sequential immunoprecipitates (IP) of surface then internal antigen using antibody against PrP^C or LRP1. The large arrow denotes the major 37-kDa di-glycosylated surface form of PrP^C, the mid-size arrow shows monoglycosylated PrP^C, and the small arrow shows non-glycosylated 23-kDa PrP^C. PrP immunoblots are from the same gel, with duplicate samples run separately for Thy-1. (B) Immunoprecipitates for internal PrP or LRP1 (from part A) were diluted in endo H digestion buffer and either digested or not with the glycosidase, as indicated, before being immunoblotted for PrP. Arrows denote the relevant PrP^C glycoforms as in A; the asterisk denotes the (slanted) band of endo H enzyme that binds antibodies nonspecifically.

seen following LRP1 downregulation by prolonged $siRNA^{LRP1}$-treatment, including the accumulation of excess PrP^C primarily in post-ER compartments (Table 3). In the case of Tg20 neurons, however, there is no elevation in BiP levels (*P*=0.47; supplementary material Table S6b).

LRP1 and PrP^C interact on the surface and within biosynthetic compartments of normal sensory neurons

To assess biochemically whether PrP^C could interact with LRP1 on the cell surface and in intracellular compartments of normal, untreated sensory neurons, LRP1 was sequentially immunoprecipitated from the surface, and then from internal compartments, of these cells (Fig. 8A). A subset of surface PrP^C co-immunoprecipitated with LRP1 (Fig. 8A, lane 2 compared with lane 1). There was no co-immunoprecipitation of Thy-1, the major neuronal GPI-anchored surface protein with PrP^C or LRP1 (lanes 1′and 2′; total Thy-1 is in the unbound fractions, lanes 5′ and 6′).

The major proportion of PrP^C on the sensory neurons was immunoprecipitated from internal compartments (Fig. 8A, lane 3 compared with lane 1, with unbound PrP^C shown in lane 5). A substantial proportion of internal PrP^C co-immunoprecipitated with LRP1 (Fig. 8A, lane 4 compared with lane 3), although a major part did not (unbound fraction in lane 6).

To identify whether any of the PrP^C associated with LRP1 was in the ER, samples immunoprecipitated by antibodies against either PrP^C or LRP1 were subjected to control or endoglycosidase H (endoH) digestion and then electrophoresed and immunoblotted for PrP^C. It is difficult to discern an endoH-sensitive band within total PrP^C (Fig. 8B, lanes 1 and 2), whereas, in the proportion of PrP^C co-immunoprecipitated with LRP1, there was an increase in fully deglycosylated PrP^C after endoH treatment (Fig. 8B, lanes 3 and 4), suggesting an ER origin of part of the PrP^C bound to LRP1 in normal sensory neurons.

The N-terminal domain of PrP^C is a high affinity LRP1 ligand

As the N-terminal domain of PrP^C is flexible and does not interact structurally with the C-terminal domain (Hornemann et al., 2004), the interaction with purified human placental LRP1 of the N-terminal residues 23-107 of PrP^C, isolated as a GST fusion protein ($GST\text{-}PrP^{23\text{-}107}$), was determined by surface plasmon resonance

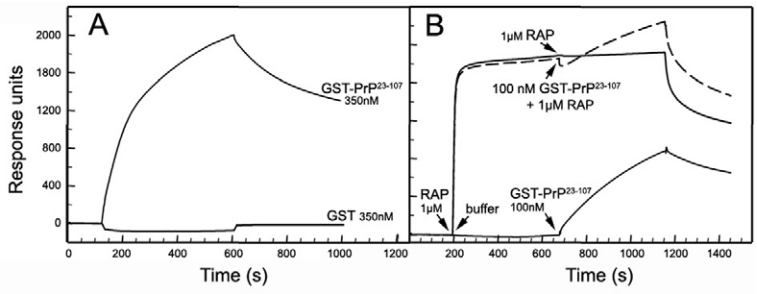

Fig. 9. Surface plasmon resonance (SPR) analysis of the binding of GST-PrP$^{23\text{-}107}$ to human LRP1. (A) Binding of 350 nM GST-PrP$^{23\text{-}107}$ compared with GST; dissociation started at 600 seconds. (B) Binding of 1 μM RAP, with a second addition of 1 μM RAP without (solid upper line) or with 100 nM GST-PrP$^{23\text{-}107}$ (dashed line); binding of 100 nM GST-PrP$^{23\text{-}107}$ alone is shown in the lower solid trace; dissociation started at 1150 seconds.

(SPR). The N-terminal domain bound with high affinity to LRP1 (Fig. 9A). The binding affinity was calculated from the estimated association (K_a=2.75×10^4 M^{-1}s^{-1}) and dissociation (K_d=5.44×10^{-4} s^{-1}) rate constants as K_D=K_d/K_a=20 nM (Fig. 9A). Similar affinities were measured in the range of 70–350 nM ligand. This binding was strongly inhibited by chelating Ca^{2+} or lowering the pH to 6.0 (data not shown), as expected for an LRP1 ligand (Fisher et al., 2006; Herz et al., 1988; Moestrup et al., 1993a). Of particular interest was the ability of PrP^C to compete with RAP. RAP at 1 μM rapidly saturated LRP1; with RAP prebound and its concentration held at 1 μM, further addition of GST-PrP$^{23\text{-}107}$ at 100 nM bound to LRP1 to 45% of its control level (Fig. 9B). This demonstrates a remarkable ability of the N-terminal domain of PrP to bind to LRP1 in the presence of its biosynthetic chaperone.

Discussion

The role of LRP1 in surface trafficking of PrP^C

The rapid and constitutive endocytosis of PrP^C on sensory neurons was inhibited by the downregulation of LRP1 by three specific siRNAs; physical association was found by co-immunoprecipitation of PrP^C and LRP1 on the neuronal surface, confirming fluorescence and EM immunocytochemical colocalisation that increased during the process of endocytosis; and the N-terminal domain of PrP^C, responsible for its endocytosis (Shyng et al., 1995a; Sunyach et al., 2003), bound with high affinity to LRP1. In addition, RAP inhibited PrP^C endocytosis, although unexpectedly high concentrations were needed; 80 nM is normally sufficient to inhibit binding of ligands to LRP1 [e.g. this concentration inhibits 90% of the binding of prion fibrils to sensory neurons (C.J.P., unpublished)], yet, in its presence, 60% of surface PrP^C was still internalised. Even at 1 μM RAP, 30% of PrP^C was still endocytosed within 2 minutes, in comparison with the 55% inhibition of GST-PrP$^{23\text{-}107}$ by this concentration of RAP. Inhibition of PrP^C by RAP occurs but is atypical for an LRP ligand. Overall, however, converging lines of evidence argue that LRP1 is the key endocytic partner of PrP^C on these neurons.

This conclusion is perhaps not unexpected, given the role of LRP1 in mediating the endocytosis of the GPI-anchored plasminogen activator receptor (Horn et al., 1998). Furthermore, Taylor and Hooper (Taylor and Hooper, 2007) reported that siRNA^{LRP1} knockdown of LRP1 inhibits the 100 μM Cu^{2+}-dependent endocytosis of exogenous transfection-expressed PrP^C on SH-SY5Y cells. These authors showed reduced internalisation of PrP^C in the presence of siRNA^{LRP1} compared with untreated cells, without testing whether their long-term siRNA^{LRP1} treatment reduced surface expression of PrP^C. In the light of our data, it would seem premature to conclude that it is the Cu^{2+}-dependent endocytosis of PrP^C, rather than its surface level, that is reduced by lowering LRP1 levels in SH-SY5Y cells.

Given the diverse roles of LRP1 in controlling neuronal lipid metabolism and surface proteins (Herz and Chen, 2006; May and Herz, 2003), separating direct from indirect effects of modulating LRP1 expression is not trivial. Not only did sustained reduction of LRP1 halve the level of surface PrP^C, it elevated Thy-1 and particularly APP levels. The latter was expected as LRP1 controls the degradation of APP (Pietrzik et al., 2004; Zerbinatti et al., 2004), but the former, not so. There is no known interaction between LRP1 and Thy-1 on the cell surface (they do not co-immunoprecipitate and, as Thy-1 is not rapidly endocytosed, they are most unlikely to interact). Possibly GPI-anchored proteins compete for a rate-limiting step in transport from the trans-Golgi to the cell surface, so that Thy-1 would benefit from lowered PrP^C traffic.

We have previously noted that the surface environment of PrP^C on neurons is complex, with PrP^C leaving its detergent-resistant domains to traverse normal (detergent soluble) membrane for endocytosis (Brügger et al., 2004; Madore et al., 1999; Sunyach et al., 2003). This complexity is evident in the colocalisation of 50% of PrP^C with the lipid 'raft' marker ganglioside GM1 (compare the ~70% distribution of PrP^C in detergent-resistant membrane) (Madore et al., 1999; Sunyach et al., 2003), and the increasing colocalisation of PrP^C with LRP1 as endocytosis progresses. We have been unable to determine whether LRP1 is within detergent-soluble or -insoluble membranes on the surface of sensory neurons because it is too readily proteolysed in detergent extracts from these cells. However, we can find no LRP1 at all within detergent-insoluble membrane fractions from brain membranes (E.G.M.V., unpublished). On myoblasts and Chinese hamster ovary (CHO) cells, LRP1 is similarly located not within detergent-resistant membranes, although it is reported to transit briefly detergent-resistant, before entering detergent-soluble, membranes for endocytosis on mouse embryonic fibroblasts (Wu and Gonias, 2005). We suspect that LRP1 does not physically enter neuronal rafts, although it might not need to in order to bind to raft-associated PrP^C as it is so large it could readily extend over the 40-100 nm diameter (Kusumi et al., 2005) of membrane rafts.

The LRP1-PrP^C interaction in vivo might limit the endocytosis of both

The size of LRP1 might lead to quite a different role for the PrP^C-LRP1 interaction in vivo from the endocytic one described here. LRP1 is so massive it could multiply-span the normal intercellular spaces of adult brain. It is more than four times larger than N-cadherin that homotypically binds to itself across the ~20 nm gap of central nervous system (CNS) synaptic clefts (Bruses, 2006; Zuber et al., 2005). In the closely packed confines of the CNS, LRP1 could bind to PrP^C on an adjacent, as readily as its own, cell surface. This would produce the opposite function to that studied in our isolated cell system – intercellular binding between PrP^C and

LRP1 presumably would prevent the endocytic trafficking of both, retaining each on the apposed surfaces until the binding of other soluble ligands (e.g. astrocyte-derived ApoE) displaced PrP^C to allow LRP1 to internalise the newly bound cargo.

This study specifically concentrated upon isolated neuronal cell bodies, devoid of attachment to other cells. Nonetheless, occasionally two neuronal cell bodies were in contact, and at such points distinct immunolabelled PrP^C remained on the surface after 2 minutes at 37°C (data not shown). The possibility that intercellular interactions between PrP^C and LRP1 stabilise both molecules to their apposed surfaces needs to be further investigated with cells in contact. Intercellular ligand binding functions have been proposed for PrP^C (e.g. Mange et al., 2002; Shmerling et al., 1998). Intercellular restriction of LRP1 trafficking by PrP^C might be particularly important at synapses, where the intracellular domain of LRP1 can organise the distribution of postsynaptic receptors through linking adaptors such as PSD95 (Herz and Chen, 2006).

Intercellular binding by LRP1-PrP^C, in restricting endocytic trafficking of both, would presumably increase the half-life of LRP1 on sensory neurons from the ~1 hour implied by our siRNA inhibition towards the 3 hours measured on HepG2 cells (Melman et al., 2002).

LRP1 as a co-receptor for PrP^C during biosynthetic transport

Members of the LRP family of receptors, each with multiple high-affinity binding sites for secreted and surface membrane proteins, form massive complexes with their ligands in the ER that prevent export to the Golgi unless their binding sites are masked by RAP (Willnow et al., 1996). This client-specific chaperone binds to nascent LRP1 as it emerges into the ER lumen (Bu and Rennke, 1996) and remains bound until LRP1 reaches the trans-Golgi (Lee et al., 2006), where the acidic (pH 5.8) environment dissociates RAP (which is retrieved by ERD2 to the ER) (Bu et al., 1997), leaving activated LRP1 to proceed to the cell surface.

LRP1 co-immunoprecipitates endoH-sensitive PrP^C from normal sensory neurons, indicating a direct interaction between these proteins in the ER. PrP^C must therefore be able to bind to LRP1 in the presence of RAP in biosynthetic compartments, a property demonstrated by SPR by the ability of GST-$PrP^{23\text{-}107}$ to bind at 45% normal capacity to LRP1 in the presence of 1 μM RAP. This, we believe, is the only reported case of a ligand binding to LRP1 in the presence of RAP. Moestrup and colleagues have extensively studied by SPR the binding kinetics of LRP family ligands. RAP has been used as a standard control and has in all previous cases completely inhibited, at 1 μM, all ligand binding (e.g. Moestrup et al., 1998; Nykjaer et al., 2001).

What is unexpected is that this interaction enhances the progress of PrP^C through biosynthetic compartments. LRP1 has been observed to promote the biosynthetic trafficking of β1 integrin to the cell surface, although direct contact between the receptor and the integrin could not be demonstrated (Salicioni et al., 2004). With levels of LRP1 reduced, high levels of PrP^C accumulated in biosynthetic compartments up to, and including, the trans-Golgi. Sustained reduction of LRP1 levels also induced high BiP levels, indicative of a stress response. However, intracellular accumulation of PrP^C was not observed by heat-shock alone, and was found with transgenic neurons with highly elevated levels of PrP^C but not LRP1 (or BiP). Taken together, these data argue for a functional role for LRP1 in expediting the biosynthetic trafficking of PrP^C.

A block in PrP^C biosynthetic trafficking at an endoH-insensitive stage occurs following deletion of N-terminal residues (23-50) (Gilch et al., 2004; Nunziante et al., 2003), following suramin-induced aggregation (Gilch et al., 2004), and with mutant forms of PrP^C that are retained in an endoH-insensitive compartment in neurons (Stewart and Harris, 2005). The LRP1-dependent block in transport seen here by lowering LRP1 levels might be a general restriction point in PrP^C biosynthesis.

Is LRP1 sufficient for neuronal trafficking of PrP^C?

We do not currently have the tools to answer this question definitively, but, from the work described here and ongoing studies, it seems highly likely that LRP1 is the central organiser, but not the sole functional component, of a larger complex that traffics PrP^C during biosynthesis and at the cell surface. We find that dissociating LRP1-PrP^C complexes is different depending on the cell source (RER microsomes versus cell surface; E.G.M.V., unpublished). Other binding partners might act as co-receptors for cellular PrP^C, decreasing its overall affinity for LRP1 sufficiently for RAP (and, presumably, other more physiologically relevant surface ligands such as ApoE) to displace PrP^C from the receptor.

Strong candidates for such a role are heparan sulphate proteoglycans (HSPGs). These bind to basic motifs in the N-terminus of PrP^C (Warner et al., 2002), affect its rate of endocytosis (Shyng et al., 1995b) and the formation of PrP^{Sc} (Ben-Zaken et al., 2003; Deleault et al., 2005). HSPGs have complex interactions with the binding and internalisation of LRP1 ligands such as thrombospondin (Wang et al., 2004) and lipoproteins (Wilsie and Orlando, 2003) and might similarly modulate the association-dissociation kinetics of LRP1-PrP^C complexes. We have noted that enzymatic removal of HSPG on sensory neurons decreases the rate of endocytosis of PrP^C (Sunyach et al., 2003).

Biological and pathological roles of the LRP1-PrP^C interaction on the cell surface

LRP1 performs two roles in internalising proteins: for nutrient uptake (particularly lipid/cholesterol), and, as a surface scavenger, removing spent debris such as protease-inhibitor complexes from the extracellular space (May and Herz, 2003). PrP^C could function as part of the LRP1 scavenger receptor complex as its N-terminal domain has multiple binding motifs (Caughey et al., 2006) and its hydrophobic sequence (residues 112-130), which is exposed to the aqueous environment, could bind to denatured proteins as PrP^C rapidly traffics across the neuronal surface. A scavenger receptor role is also suggested by the pattern of PrP^C expression in vivo, where it is most abundant on cells that might need enhanced levels of protection from the extracellular environment: on neurons, which cannot divide and live as long as the body they control, and on cells that constantly monitor danger in the environment – normal and follicular dendritic cells, intraepithelial lymphocytes and neuroendocrine cells (Ford et al., 2002a; Ford et al., 2002b).

Members of the LRP family could play multiple roles in prion infection. Infectious prion fibrils bind with picomolar affinity to very-low-density lipoproteins (Safar et al., 2006) and so might be cleared from extracellular space by LDL receptors. With neuronal LRP1, the crucial questions are whether LRP1 also binds to infectious prion fibrils and, if so, whether the same molecule of LRP1 (which binds most ligands to both cluster 2 and 4) (May and Herz, 2003) will bind to both the cellular and infectious forms of PrP? Then, given the massive size of LRP1, would such binding of the template and substrate in the prion conversion reaction bring the two together or keep them apart?

Materials and Methods

A cDNA fragment encoding residues 23-107 of PrP^C (Sunyach et al., 2003) with a C-terminal Cys residue (added to provide an anchor for conjugation) was cloned into the pGEX-4T1 vector (GE Healthcare). GST fusion protein was purified on glutathione-sepharose beads in the presence of 1 mM DTT. The Cys residue was blocked with 5 mM iodoacetamide in PBS to prevent disulphide bond formation, confirmed by recovery in non-reducing PAGE of the monomeric fusion protein without higher polymers.

Monomeric affinity-purified Fab against mouse PrP residues 142-162 (referred to as '2S antibody') was coupled to Alexa-Fluor-488 or -594 (Molecular Probes; 1–3 moles of dye per mole of Fab) or to 5 nm gold (British Biocell) as described previously (Sunyach et al., 2003). To detect PrP on immunoblots or for immunocytochemistry of fixed cells, SAF32 and SAF83 (SPI-Bio Massy, France) monoclonal antibodies against PrP were used, directly coupled to fluorochromes or gold for immunocytochemistry. Mouse monoclonals to syntaxin 6 (Abcam) and α-mannosidase II (Covance), the LRP1 ligand α_2M* (Research Diagnostics) and cholera toxin B chain (Sigma) were coupled to fluorochromes, as described above. Fe^{2+}-loaded transferrin (Tf) coupled to Alexa-Fluor-488 or Texas Red was from Molecular Probes; both ligands were used at 50 μg/ml.

For detection of LRP1, rabbit antibodies against the entire LRP1 (RRR) (Bu et al., 1995), or its cytoplasmic domain (MMMM) (Zerbinatti et al., 2004), were used; LRP1b was detected with an anti-epitope antibody (Cam et al., 2004). Rabbit antibodies against other neuronal LRP family members (LRP6, LRP8, VLDLR) were from Santa Cruz, and against BiP were from Abcam (ab21685). Rabbit antibodies were detected with our own affinity-purified, species-specific horse anti-rabbit IgG conjugated to Alexa fluorochromes, as described above.

Surface plasmon resonance

To study the binding of GST-PrP^{23-107} to LRP1 by SPR on a Biacore 3000 (Biacore, Sweden), CM5 sensor chips were activated with a 1:1 mixture of 0.2 M *N*-ethyl-*N*′-(3-dimethylaminopropyl) carbodiimide and 0.05 M *N*-hydroxysuccimide in water. LRP1, purified from human placenta (Moestrup et al., 1993a), was immobilised at a concentration 15 μg/ml in 10 mM sodium acetate pH 3.0, to a receptor density of 20-30 fmol LRP/mm^2. Remaining binding sites were blocked with 1 M ethanolamine pH 8.5. A control flow cell was made by performing the activation and blocking procedure only. Samples were dissolved in 10 mM HEPES, 150 mM NaCl, 1.5 mM $CaCl_2$, 1 mM EGTA, pH 7.4 plus 0.005% Tween 20. Sample and running buffers were identical. Samples were injected at a flow rate of 5 μl/minute. Regeneration of the sensor chip after each analysis cycle was performed with 1.6 M glycine-HCl buffer, pH 3.0. The Biacore response is expressed in relative response units (RU), this being the difference in response between the protein and control flow channel. Kinetic parameters were determined by BIAevaluation 4.1 software using a Langmuir 1:1 binding model and simultaneous fitting of all curves in the concentration range.

Sensory neurons and PrP^C internalisation

Neurons were used after 3-7 days in culture established from the dorsal root ganglia of 4-8-week-old 129Sv, or Tg20 transgenic (Fischer et al., 1996), mice (*Mus musculus*) or (for biochemistry) rats (*Rattus norvegicus*) (Sunyach et al., 2003). Genetically normal rat and mouse neurons endocytosed their endogenous PrP^C at the same rate and were inhibited by the $siRNA^{LRP1}$ used with similar efficiency.

For siRNA delivery by penetratin-1 (Davidson et al., 2004; Dom et al., 2003), all extracellular DNA was removed by treating cultures overnight with RNAse-free DNAse (5 units/ml; Qiagen) and including the enzyme in the incubation with siRNA-penetratin.

Endocytosis assays were performed as described previously (Sunyach et al., 2003). Briefly, cells were prelabelled with ligands for 30 minutes at 10-12°C in B-27 supplement-free medium, washed once and transferred to a 37°C incubator for endocytosis, normally for 0-2 minutes. At timed intervals, samples were fixed with 1.5% PFA for 15 minutes, chromatin stained with 4′,6 diamidino-2-phenylindole (DAPI), and mounted in mowiol. Cells were observed with a Zeiss Axiovert 100 microscope with a piezo *Z*-axis drive on a 63× apochromat 1.4 NA oil objective illuminated with an EXFO X-cite 120 metal-halide lamp and images collected with a Hamamatsu Orca-ER camera. Exposure time (50-500 mseconds) and excitation intensity were set so that points of highest light intensity were within 20-60% saturation for the camera. Images (normally 30) taken every 100 nm through a middle section of the cell body [to obtain multiple data points per wavelength in the *Z* axis (Heintzmann, 2005)] were transferred to Volocity (Improvision; Warwick, UK), subtractively deconvolved against their seven neighbouring images, assembled into a 3D stack and fluorescence measured using Volocity. Background was set at 10% above the level that resolved the measured fluorescence into multiple discrete objects (rather than record the whole cell as a single fluorescent object). Surface objects were defined by drawing a line just below the surface of each cell.

For EM, gold was labeled with Fab, Tf or α_2M* and incubated with cells and processed for EM as described previously (Sunyach et al., 2003). Fields of both PrP^C-α_2M* and PrP^C-Tf double labeling were viewed to count >500 particles of 5 nm gold labeling for PrP^C, and the proximity to them of the 10 nm label for the other two ligands determined. Label for the LRP1 ligand α_2M* was present at 80%, and that for Tf at 60%, the abundance of label for PrP^C. The relative density of the α_2M* and Tf labels was similar (respectively 80% and 60% the density of PrP^C label), as was the fraction of label for all three within coated pits (11-18%).

Immunocytochemical labeling

To assess surface immunolabelling, where the relative distribution of surface proteins was crucial (Fig. 2C,D; Table 1), neurons were kept at 37°C as they were washed in PBS and fixed for 15 minutes with 0.5% PFA, then immunolabelled at 4°C. Where the amount rather than surface distribution of surface protein was crucial, living cells were immunolabeled at 10°C, then fixed in 0.5% PFA for 15 minutes. If internal protein was also to be measured, cells were permeabilised at 4°C in Brij-96–PBS for 30 minutes, then internal protein was immunolabelled. Cells were DAPI stained, fixed again in 1.5% PFA-PBS for 1-16 hours before being mounted in mowiol. If primarily internal proteins were to be labeled (e.g. Fig. 6), cells were fixed for 30 minutes with 1.5% PFA at room temperature, then permeabilised for 30 minutes at 4°C in 0.2% Triton-X-100–PBS before immunolabelling. Mowiol moutant was made in PBS containing 1/7 by volume mowiol 4-88, 2/7 glycerol, 0.1% NaN_3, 0.1 mg/ml DABCO [1,4 diazabizyclo(2.2.2)octane] and 0.01 mg/ml n-propyl gallate (all from Sigma).

Inhibition of LRP1: RAP and siRNA

Recombinant RAP (80 nM or 1 μM) (Andersen et al., 2001) was preincubated with cells for 30–60 minutes at 37°C before the PrP internalisation assay was performed. The $siRNA^{LRP1.1}$ sequence was adapted for the mouse from the human sequence that we have found to be effective in suppressing LRP1 in human smooth muscle cells (Li et al., 2003); sense strand Th-5′-GCAGUUUGCCUGCAGAGAGdTdT-3′, antisense strand 5′UCUCGCAGGCAAACUGCdTdT-3′). The control $siRNA^{Con}$ corresponded to the reverse of the $siRNA^{LRP1}$ sequence. NCBI Blastn showed that the $siRNA^{LRP1.1}$ would only target mRNA encoding Lrp1 and that there would be no target for $siRNA^{Con}$. In addition, $siRNA^{LRP1.2}$ (sense strand Th-5′-CGUUGGUU-AUGCACAUGAAdTdT-3′, antisense strand 5′UUCAUGUGCAUAACCA-ACGdTdT-3′), and $siRNA^{LRP1.3}$ (sense strand Th-5′-GCCGGGUGUACAAAUGU-AAdTdT-3′, antisense strand 5′UUACAUUUGUACACCCGGCdTdT-3′) were predesigned and homology tested using proprietary algorithms by the manufacturer (Qiagen). The appropriate thio-modified double-stranded RNAs (Dharmacon and Qiagen) were coupled to penetratin-1 (Quantum Biotechnologies) following Davidson and colleagues (Davidson et al., 2004) and added to cells at a final concentration of 250 nM.

Immunoprecipitation

For sequential immunoprecipitation of surface then intracellular antigen, antibody [SAF32 (1 μg) for PrP^C; RRR (3 μg) for LRP1; Ox7 (1 μg) for Thy-1] was added to 1.5 ml of culture medium and neurons held at 10°C for 30 minutes with gentle rocking before being washed twice in ice-cold PBS and recovered from the plate by aspiration. Cells were lysed in 0.5% Brij 96 plus 0.5% sodium deoxycholate plus 1 μM BSA. Nuclei were pelleted at 2400 ***g*** for 5 minutes, and protein A Dynal beads (10% v/v) were incubated with the supernatant for 30 minutes at 4°C, then washed with lysis buffer, and antigen eluted using Laemmli SDS-PAGE sample buffer.

Internal antigen was then immunoprecipitated by incubating the unbound fraction with primary antibodies followed by protein A Dynal beads and eluted with 0.1% SDS in 10 mM Tris pH 6.8 for digestion with endoglycosidase H (endoH).

For hydrolysis of core glycan chains with endoH, samples were reduced with 10 mM DTT for 5 minutes at 100°C, diluted twofold in 0.5 M citrate buffer pH 5.5 plus 0.1 mM EDTA and endoH (Roche) added at 0.1 U/ml for 60 minutes at 37°C. The reaction was stopped by boiling samples in Laemmli sample buffer.

We thank Carol Troy (Columbia, NY) for advice on coupling and use of penetratin-siRNA, Charles Weissmann for the Tg20 mice, Ken Brady (Centre for Ultrastructural Imaging, King's College London, UK) for expert assistance with the EM, and Maria Woolston for positive controls for antibodies against the LRP family; we also thank Helen Cox, Paul Felts and Susan Standring for many useful discussions, and Improvision for continuing support. This work was supported by BBSRC grants 18/BS516350 and BB/C506680/1. We also acknowledge the reviewers for their incisive, constructive comments that have much improved this paper. This work was supported by BBSRC grants 18/BS516350 and BB/C506680/1, and an MRC doctoral training studentship to C.J.P.

References

Andersen, O. M., Schwarz, F. P., Eisenstein, E., Jacobsen, C., Moestrup, S. K., Etzerodt, M. and Thogersen, H. C. (2001). Dominant thermodynamic role of the third independent receptor binding site in the receptor-associated protein RAP. *Biochemistry* **40**, 15408-15417.

Ben-Zaken, O., Tzaban, S., Tal, Y., Horonchik, L., Esko, J. D., Vlodavsky, I. and Taraboulos, A. (2003). Cellular heparan sulfate participates in the metabolism of prions. *J. Biol. Chem.* **278**, 40041-40049.

Brügger, B., Graham, C. H., Leibrecht, I., Mombelli, E., Jen, A., Wieland, F. T. and Morris, R. J. (2004). The membrane domains occupied by glycosylphosphatidylinositol-anchored prion protein and Thy-1 differ in lipid composition. *J. Biol. Chem.* **279**, 7530-7536.

Bruses, J. L. (2006). N-cadherin signaling in synapse formation and neuronal physiology. *Mol. Neurobiol.* **33**, 237-252.

Bu, G. and Rennke, S. (1996). Receptor-associated protein is a folding chaperone for low density lipoprotein receptor-related protein. *J. Biol. Chem.* **271**, 22218-22224.

Bu, G., Maksymovitch, E. A., Nerbonne, J. M. and Schwartz, A. L. (1994). Expression and function of the low density lipoprotein receptor-related protein (LRP) in mammalian central neurons. *J. Biol. Chem.* **269**, 18521-18528.

Bu, G., Geuze, H. J., Strous, G. J. and Schwartz, A. L. (1995). 39 kDa receptor-associated protein is an ER resident protein and molecular chaperone for LDL receptor-related protein. *EMBO J.* **14**, 2269-2280.

Bu, G., Rennke, S. and Geuze, H. J. (1997). ERD2 proteins mediate ER retention of the HNEL signal of LRP's receptor-associated protein (RAP). *J. Cell Sci.* **110**, 65-73.

Cam, J. A., Zerbinatti, C. V., Knisely, J. M., Hecimovic, S., Li, Y. and Bu, G. (2004). The low density lipoprotein receptor-related protein 1B retains beta-amyloid precursor protein at the cell surface and reduces amyloid-beta peptide production. *J. Biol. Chem.* **279**, 29639-29646.

Caughey, B., Caughey, W. S., Kocisko, D. A., Lee, K. S., Silveira, J. R. and Morrey, J. D. (2006). Prions and transmissible spongiform encephalopathy (TSE) chemotherapeutics: a common mechanism for anti-TSE compounds? *Acc. Chem. Res.* **39**, 646-653.

Davidson, T. J., Harel, S., Arboleda, V. A., Prunell, G. F., Shelanski, M. L., Greene, L. A. and Troy, C. M. (2004). Highly efficient small interfering RNA delivery to primary mammalian neurons induces MicroRNA-like effects before mRNA degradation. *J. Neurosci.* **24**, 10040-10046.

Deleault, N. R., Geoghegan, J. C., Nishina, K., Kascsak, R., Williamson, R. A. and Supattapone, S. (2005). Protease-resistant prion protein amplification reconstituted with partially purified substrates and synthetic polyanions. *J. Biol. Chem.* **280**, 26873-26879.

Dom, G., Shaw-Jackson, C., Matis, C., Bouffioux, O., Picard, J. J., Prochiantz, A., Mingeot-Leclercq, M. P., Brasseur, R. and Rezsohazy, R. (2003). Cellular uptake of Antennapedia Penetratin peptides is a two-step process in which phase transfer precedes a tryptophan-dependent translocation. *Nucleic Acids Res.* **31**, 556-561.

Fischer, M., Rülicke, T., Raeber, A., Sailer, A., Moser, M., Oesch, B., Brandner, S., Aguzzi, A. and Weissmann, C. (1996). Prion protein (PrP) with amino-proximal deletions restoring susceptibility of PrP knockout mice to scrapie. *EMBO J.* **15**, 1255-1264.

Fisher, C., Beglova, N. and Blacklow, S. C. (2006). Structure of an LDLR-RAP complex reveals a general mode for ligand recognition by lipoprotein receptors. *Mol. Cell* **22**, 277-283.

Ford, M. L., Burton, L. J., Li, H., Graham, C. H., Frobert, Y., Grassi, J., Hall, S. M. and Morris, R. J. (2002a). A marked disparity between the expression of prion protein and its message by neurons of the central nervous system. *Neuroscience* **111**, 533-551.

Ford, M. L., Burton, L. J., Morris, R. J. and Hall, S. M. (2002b). Selective expression of prion protein in peripheral tissues of the adult mouse. *Neuroscience* **113**, 177-192.

Gauczynski, S., Peyrin, J. M., Haik, S., Leucht, C., Hundt, C., Rieger, R., Krasemann, S., Deslys, J. P., Dormont, D., Lasmezas, C. I. et al. (2001). The 37-kDa/67-kDa laminin receptor acts as the cell-surface receptor for the cellular prion protein. *EMBO J.* **20**, 5863-5875.

Gilch, S., Nunziante, M., Ertmer, A., Wopfner, F., Laszlo, L. and Schatzl, H. M. (2004). Recognition of lumenal prion protein aggregates by post-ER quality control mechanisms is mediated by the preoctarepeat region of PrP. *Traffic* **5**, 300-313.

Heintzmann, R. (2005). Band limit and appropriate sampling in microscopy. In *Cell Biology: A Laboratory Handbook* (ed. K. Simons, J. V. Small, T. Hunter, D. Shotton, J. E. Celis and N. Carter), pp. 29-36. Amsterdam: Elsevier.

Herz, J. and Chen, Y. (2006). Reelin, lipoprotein receptors and synaptic plasticity. *Nat. Rev. Neurosci.* **7**, 850-859.

Herz, J., Hamann, U., Rogne, S., Myklebost, O., Gausepohl, H. and Stanley, K. K. (1988). Surface location and high affinity for calcium of a 500-kd liver membrane protein closely related to the LDL-receptor suggest a physiological role as lipoprotein receptor. *EMBO J.* **7**, 4119-4127.

Horn, I. R., van den Berg, B. M., Moestrup, S. K., Pannekoek, H. and van Zonneveld, A. J. (1998). Plasminogen activator inhibitor 1 contains a cryptic high affinity receptor binding site that is exposed upon complex formation with tissue-type plasminogen activator. *Thromb. Haemost.* **80**, 822-828.

Hornemann, S., Schorn, C. and Wuthrich, K. (2004). NMR structure of the bovine prion protein isolated from healthy calf brains. *EMBO Rep.* **5**, 1159-1164.

Iadonato, S. P., Bu, G., Maksymovitch, E. A. and Schwartz, A. L. (1993). Interaction of a 39 kDa protein with the low-density-lipoprotein-receptor-related protein (LRP) on rat hepatoma cells. *Biochem. J.* **296**, 867-875.

Kazmin, D. A., Chinenov, Y., Larson, E. and Starkey, J. R. (2003). Comparative modeling of the N-terminal domain of the 67kDa laminin-binding protein: implications for putative ribosomal function. *Biochem. Biophys. Res. Commun.* **300**, 161-166.

Kusumi, A., Nakada, C., Ritchie, K., Murase, K., Suzuki, K., Murakoshi, H., Kasai, R. S., Kondo, J. and Fujiwara, T. (2005). Paradigm shift of the plasma membrane concept from the two-dimensional continuum fluid to the partitioned fluid: high-speed single-molecule tracking of membrane molecules. *Annu. Rev. Biophys. Biomol. Struct.* **34**, 351-378.

Lee, D., Walsh, J. D., Mikhailenko, I., Yu, P., Migliorini, M., Wu, Y., Krueger, S., Curtis, J. E., Harris, B., Lockett, S. et al. (2006). RAP uses a histidine switch to regulate its interaction with LRP in the ER and Golgi. *Mol. Cell* **22**, 423-430.

Li, Y., Marzolo, M. P., van Kerkhof, P., Strous, G. J. and Bu, G. (2000). The YXXL motif, but not the two NPXY motifs, serves as the dominant endocytosis signal for low density lipoprotein receptor-related protein. *J. Biol. Chem.* **275**, 17187-17194.

Li, Y., Lu, W. and Bu, G. (2003). Essential role of the low density lipoprotein receptor-related protein in vascular smooth muscle cell migration. *FEBS Lett.* **555**, 346-350.

Linden, R., Martins, V. R., Prado, M. A., Izquierdo, I. and Brentani, R. R. (2008). Physiology of the prion protein. *Physiol. Rev.* In press.

Madore, N., Smith, K. L., Graham, C. H., Jen, A., Brady, K., Hall, S. and Morris, R. (1999). Functionally different GPI proteins are organised in different domains on the neuronal surface. *EMBO J.* **18**, 6917-6926.

Mange, A., Milhavet, O., Umlauf, D., Harris, D. and Lehmann, S. (2002). PrP-dependent cell adhesion in N2a neuroblastoma cells. *FEBS Lett.* **514**, 159-162.

Mauch, D. H., Nagler, K., Schumacher, S., Goritz, C., Muller, E. C., Otto, A. and Pfrieger, F. W. (2001). CNS synaptogenesis promoted by glia-derived cholesterol. *Science* **294**, 1354-1357.

May, P. and Herz, J. (2003). LDL receptor-related proteins in neurodevelopment. *Traffic* **4**, 291-301.

May, P., Rohlmann, A., Bock, H. H., Zurhove, K., Marth, J. D., Schomburg, E. D., Noebels, J. L., Beffert, U., Sweatt, J. D., Weeber, E. J. et al. (2004). Neuronal LRP1 functionally associates with postsynaptic proteins and is required for normal motor function in mice. *Mol. Cell. Biol.* **24**, 8872-8883.

Melman, L., Geuze, H. J., Li, Y., McCormick, L. M., Van Kerkhof, P., Strous, G. J., Schwartz, A. L. and Bu, G. (2002). Proteasome regulates the delivery of LDL receptor-related protein into the degradation pathway. *Mol. Biol. Cell* **13**, 3325-3335.

Moestrup, S. K., Gliemann, J. and Pallesen, G. (1992). Distribution of the alpha 2-macroglobulin receptor/low density lipoprotein receptor-related protein in human tissues. *Cell Tissue Res.* **269**, 375-382.

Moestrup, S. K., Holtet, T. L., Etzerodt, M., Thogersen, H. C., Nykjaer, A., Andreasen, P. A., Rasmussen, H. H., Sottrup-Jensen, L. and Gliemann, J. (1993a). Alpha 2-macroglobulin-proteinase complexes, plasminogen activator inhibitor type-1-plasminogen activator complexes, and receptor-associated protein bind to a region of the alpha 2-macroglobulin receptor containing a cluster of eight complement-type repeats. *J. Biol. Chem.* **268**, 13691-13696.

Moestrup, S. K., Nielsen, S., Andreasen, P., Jorgensen, K. E., Nykjaer, A., Roigaard, H., Gliemann, J. and Christensen, E. I. (1993b). Epithelial glycoprotein-330 mediates endocytosis of plasminogen activator-plasminogen activator inhibitor type-1 complexes. *J. Biol. Chem.* **268**, 16564-16570.

Moestrup, S. K., Schousboe, I., Jacobsen, C., Leheste, J. R., Christensen, E. I. and Willnow, T. E. (1998). beta2-glycoprotein-I (apolipoprotein H) and beta2-glycoprotein-I-phospholipid complex harbor a recognition site for the endocytic receptor megalin. *J. Clin. Invest.* **102**, 902-909.

Morris, R. J., Parkyn, C. J. and Jen, A. (2006). Traffic of prion protein between different compartments on the neuronal surface, and the propagation of prion disease. *FEBS Lett.* **580**, 5565-5571.

Nunziante, M., Gilch, S. and Schatzl, H. M. (2003). Essential role of the prion protein N terminus in subcellular trafficking and half-life of cellular prion protein. *J. Biol. Chem.* **278**, 3726-3734.

Nykjaer, A., Fyfe, J. C., Kozyraki, R., Leheste, J. R., Jacobsen, C., Nielsen, M. S., Verroust, P. J., Aminoff, M., de la Chapelle, A., Moestrup, S. K. et al. (2001). Cubilin dysfunction causes abnormal metabolism of the steroid hormone 25(OH) vitamin D(3). *Proc. Natl. Acad. Sci. USA* **98**, 13895-13900.

Peters, P. J., Mironov, A., Jr, Peretz, D., van Donselaar, E., Leclerc, E., Erpel, S., DeArmond, S. J., Burton, D. R., Williamson, R. A., Vey, M. et al. (2003). Trafficking of prion proteins through a caveolae-mediated endosomal pathway. *J. Cell Biol.* **162**, 703-717.

Pietrzik, C. U., Yoon, I. S., Jaeger, S., Busse, T., Weggen, S. and Koo, E. H. (2004). FE65 constitutes the functional link between the low-density lipoprotein receptor-related protein and the amyloid precursor protein. *J. Neurosci.* **24**, 4259-4265.

Safar, J. G., Wille, H., Geschwind, M. D., Deering, C., Latawiec, D., Serban, A., King, D. J., Legname, G., Weisgraber, K. H., Mahley, R. W. et al. (2006). Human prions and plasma lipoproteins. *Proc. Natl. Acad. Sci. USA* **103**, 11312-11317.

Salicioni, A. M., Gaultier, A., Brownlee, C., Cheezum, M. K. and Gonias, S. L. (2004). Low density lipoprotein receptor-related protein-1 promotes beta1 integrin maturation and transport to the cell surface. *J. Biol. Chem.* **279**, 10005-10012.

Scott, B. S. (1977). Adult mouse dorsal root ganglia neurons in cell culture. *J. Neurobiol.* **8**, 417-427.

Shmerling, D., Hegyi, I., Fischer, M., Blattler, T., Brandner, S., Gotz, J., Rulicke, T., Flechsig, E., Cozzio, A., von Mering, C. et al. (1998). Expression of amino-terminally truncated PrP in the mouse leading to ataxia and specific cerebellar lesions. *Cell* **93**, 203-214.

Shyng, S.-L., Heuser, J. E. and Harris, D. A. (1994). A glycolipid-anchored prion protein is endocytosed via clathrin-coated pits. *J. Cell Biol.* **125**, 1239-1250.

Shyng, S.-L., Moulder, K. L., Lesko, A. and Harris, D. A. (1995a). The N-terminal domain of a glycolipid-anchored prion protein is essential for its endocytosis via clathrin-coated pits. *J. Biol. Chem.* **270**, 14793-14800.

Shyng, S. L., Lehmann, S., Moulder, K. L. and Harris, D. A. (1995b). Sulfated glycans stimulate endocytosis of the cellular isoform of the prion protein, PrPC, in cultured cells. *J. Biol. Chem.* **270**, 30221-30229.

Springer, T. A. (1998). An extracellular beta-propeller module predicted in lipoprotein and scavenger receptors, tyrosine kinases, epidermal growth factor precursor, and extracellular matrix components. *J. Mol. Biol.* **283**, 837-862.

Stewart, R. S. and Harris, D. A. (2005). A transmembrane form of the prion protein is localized in the Golgi apparatus of neurons. *J. Biol. Chem.* **280**, 15855-15864.

Sunyach, C., Jen, A., Deng, J., Fitzgerald, K., Frobert, Y., McCaffrey, M. and Morris, R. J. (2003). The mechanism of internalisation of GPI anchored prion protein. *EMBO J.* **22**, 3591-3601.

Taylor, D. R. and Hooper, N. M. (2007). The low-density lipoprotein receptor-related protein 1 (LRP1) mediates the endocytosis of the cellular prion protein. *Biochem. J.* **402**, 17-23.

Wang, S., Herndon, M. E., Ranganathan, S., Godyna, S., Lawler, J., Argraves, W. S. and Liau, G. (2004). Internalization but not binding of thrombospondin-1 to low density lipoprotein receptor-related protein-1 requires heparan sulfate proteoglycans. *J. Cell. Biochem.* **91**, 766-776.

Warner, R. G., Hundt, C., Weiss, S. and Turnbull, J. E. (2002). Identification of the heparan sulphate binding sites in the cellular prion protein. *J. Biol. Chem.* **277**, 18421-18430.

Willnow, T. E., Rohlmann, A., Horton, J., Otani, H., Braun, J. R., Hammer, R. E. and Herz, J. (1996). RAP, a specialized chaperone, prevents ligand-induced ER retention and degradation of LDL receptor-related endocytic receptors. *EMBO J.* **15**, 2632-2639.

Wilsie, L. C. and Orlando, R. A. (2003). The low density lipoprotein receptor-related protein complexes with cell surface heparan sulfate proteoglycans to regulate proteoglycan-mediated lipoprotein catabolism. *J. Biol. Chem.* **278**, 15758-15764.

Wu, L. and Gonias, S. L. (2005). The low-density lipoprotein receptor-related protein-1 associates transiently with lipid rafts. *J. Cell. Biochem.* **96**, 1021-1033.

Zerbinatti, C. V., Wozniak, D. F., Cirrito, J., Cam, J. A., Osaka, H., Bales, K. R., Zhuo, M., Paul, S. M., Holtzman, D. M. and Bu, G. (2004). Increased soluble amyloid-beta peptide and memory deficits in amyloid model mice overexpressing the low-density lipoprotein receptor-related protein. *Proc. Natl. Acad. Sci. USA* **101**, 1075-1080.

Zuber, B., Nikonenko, I., Klauser, P., Muller, D. and Dubochet, J. (2005). The mammalian central nervous synaptic cleft contains a high density of periodically organized complexes. *Proc. Natl. Acad. Sci. USA* **102**, 19192-19197.

Journal of Cell Science

Table S1a: extent of co-localization of PrP and LRP1 during endocytosis (for Table 1 in paper)

		Fluorescence Intensity (arbitrary units)				Calculated %ages			
	Cell	**Surface PrP**	**Surface LRP**	**PrP colocalize with LRP**	**LRP colocalize with PrP**	**% of PrP colocalize with LRP**	**% LRP Co-localized with PrP**	**% endocy of PrP**	**% PrP on Surface**
0 minutes	C-1	424,204	290,387	121,696	103,996	28.7%	35.8%	0.0%	100.0%
	C-11	114,301	78,799	29,694	19,421	26.0%	24.6%	25.3%	74.7%
	C-2	351,892	481,473	131,257	150,670	37.3%	31.3%	0.0%	100.0%
	C-5	129,338	90,085	56,560	40,149	43.7%	44.6%	26.2%	73.8%
	C-7	158,598	58,506	86,115	32,609	54.3%	55.7%	3.4%	96.6%
	C-8	179,155	21,473	28,797	15,361	16.1%	71.5%	37.4%	62.6%
	C-9	151,095	179,478	116,743	74,245	77.3%	41.4%	20.6%	79.4%
	C-10	265,821	260,051	109,582	105,039	41.2%	40.4%	27.5%	72.5%
					Average	**40.6%**	**43.2%**	17.6%	**82.4%**
					s.d.	18.9%	14.7%	14.4%	14.4%
1 minute	1'-1	146,024	2,867,490	101,114	632,543	69.2%	22.1%	28.4%	71.6%
	1'-2	152,276	731,520	72,138	256,746	47.4%	35.1%	19.3%	80.7%
	1'-1b	102,345	1,845,110	68,677	455,721	67.1%	24.7%	3.2%	96.8%
	1'-3	64,974	340,648	52,311	56,908	80.5%	16.7%	73.3%	26.7%
	1'-4	173,971	407,457	84,461	194,658	48.5%	47.8%	73.6%	26.4%
	1'10	106,791	147,536	79,163	106,841	74.1%	72.4%	69.3%	30.7%
	1'-11	119,368	166,829	51,225	104,907	42.9%	62.9%	73.3%	26.7%
	1'-12	27,561	107,876	12,701	22,874	46.1%	21.2%	91.7%	8.3%
	1'-9	93,782	208,027	60,740	103,096	64.8%	49.6%	82.7%	17.3%
					Average	**60.1%**	**39.2%**	57.2%	**42.8%**
					s.d.	13.9%	20.0%	31.5%	31.5%
					Differs from 0 minute , p=	0.01	0.27		
2 minutes	4-1	361,790		357,200		98.7%		77.3%	22.7%
	4-2	382,429		376,203		98.4%		79.8%	20.2%
	4-3	108,980		106,680		97.9%		94.8%	5.2%
	4-4	124,727		124,069		99.5%		91.8%	8.2%
	5-1	322,458		314,092		97.4%		83.0%	17.0%
	5-2	120,970		119,279		98.6%		93.2%	6.8%
	5-3	71,423		70,300		98.4%		95.9%	4.1%
	3-1	275,105		270,518		98.3%		85.4%	14.6%
	3-2	225,111		221,864		98.6%		90.5%	9.5%
	3-3	135,193		133,770		98.9%		93.6%	6.4%
	2-6	18,701		16,427		87.8%		88.2%	11.8%
	2-1	91,855		90,514		98.5%		76.2%	23.8%
	2.2	206,363		203,256		98.5%		84.5%	15.5%
	2.3	303,375		299,288		98.7%		78.9%	21.1%
					Average	**97.7%**		86.7%	**13.3%**
					s.d.	2.9%		6.9%	6.9%
					Differs from 0 minute , p=	0.00005		0.000001	0.000001

Table S1b: extent of co-localization of PrP with Ctx on neuronal surface (for Fig. 2D in paper)

Cell	PrP total	Ctx total	PrP/Ctx	Ctx/PrP	% PrP/Ctx	% Ctx/PrP
c2.1	218,007	672,059	121,710	388,467	55.8%	57.8%
C3.2	111,502	321,443	42,068	156,297	37.7%	48.6%
C3	600,211	650,944	165,027	523,352	27.5%	80.4%
C5	718,678	2,363,070	553,101	1,691,990	77.0%	71.6%
C4	164,733	127,902	57,642	83,538	35.0%	65.3%
2S	37,013	163,619	23,448	123,323	63.4%	75.4%
c7	785,330	5,881,140	653,679	2,669,690	83.2%	45.4%
				Average	**54.2%**	**63.5%**
				s.d.	21.6%	13.4%

Table S2a: RAP inhibition at 1 μM

Cell	% PrP endocytosed	% Tf endocytosed
cell+RAP-01	25.28	96.48
cell+RAP-02	73.73	99.04
cell+RAP-03	26.42	97.01
cell+RAP-04	25.44	98.50
cell+RAP-05	12.48	91.50
cell+RAP-06	12.24	92.66
cell+RAP-07	13.74	96.83
cell+RAP-08	9.44	91.59
cell+RAP-09	28.22	94.06
cell+RAP-10	26.57	91.93
cell+RAP-11	6.18	94.71
cell+RAP-12	70.86	96.03
cell+RAP-13	24.84	91.06
cell+RAP-13a	47.46	91.57
cell+RAP-14	24.45	93.94
cell+RAP-15	38.29	94.37
Mean	**29.10**	**94.45**
s.d.	19.28	2.54
Ttest, p=	**4.49561E-10**	**0.527**
cell-01	93.18	100.00
cell-02	96.31	91.55
cell-04	92.89	98.22
cell-06	99.60	81.25
cell-07	90.04	88.85
cell-08	92.98	95.58
cell-09	95.20	90.73
cell-10	85.31	97.42
Mean	**93.19**	**92.95**
s.d.	4.26	6.15

Table S2b: RAP inhibition at 80 nM (one of 4 exps)

Cell	% PrP endocytosed	% Tf endocytosed
cell-01 (controls)	81.0	90.0
cell-02	81.4	95.5
cell-04	84.7	91.5
cell-05	74.8	84.4
cell-06	90.0	97.7
cell-07	87.4	86.5
cell-09	89.2	99.0
cell-10	79.6	78.6
cell-12	87.0	80.5
cell-13	71.2	89.1
cell-14	71.6	89.4
cell-15	77.9	76.0
mean	**75.1**	**88.17**
s.d.	**6.54**	7.36
cell-02+RAP	33.9	90.0
cell-03+RAP	55.1	95.5
cell-05+RAP	50.6	91.5
cell-06+RAP	54.5	84.4
cell-09+RAP	58.8	97.7
cell-10+RAP	55.6	86.5
cell-12+RAP	62.1	99.0
mean	**52.93**	**92.08**
s.d.	9.13	5.58
Ttest, p =	**0.00003**	**0.21**

Table S2c: example of calculation of levels of surface PrP and LRP1 after 90 minutes treatment with siRNA

Cell	Cell Volume µm3	LRP1 fluorescence intensity	PrP fluorescence intensity	LRP1 intensity per µm3	PrP intensity per µm3
LRP1.1 siRNA	343	8,397,390	195,056	24,482	569
	1659	12,676,000	720,599	7,641	434
	348	5,851,720	125,121	16,815	360
	782	15,878,000	1,144,690	20,304	1,464
	435	6,358,980	299,884	14,618	689
	2149	23,786,900	32,421	11,069	15
	377	5,600,830	373,391	14,856	990
	512	6,879,960	379,357	13,437	741
	1001	17,418,300	809,290	17,401	808
	769	20,051,100	338,069	26,074	440
	452	6,247,620	172,785	13,822	382
	493	10,489,900	673,987	21,278	1,367
Average				**16,817**	**688**
s.d.				5,189	405
% of control				**64.0%**	**107.3%**
Control siRNA	578	19,989,800	203,825	34,584	353
	550	11,882,300	90,571	21,604	165
	552	10,794,200	697,103	19,555	1,263
	214	6,425,750	73,060	30,027	341
	664	25,360,600	477,038	38,194	718
	1169	25,102,900	732,942	21,474	627
	442	17,942,700	1,030,370	40,594	2,331
	325	8,665,440	470,610	26,663	1,448
	307	5,563,810	124,707	18,123	406
	532	12,527,600	77,118	23,548	145
	443	6,139,400	111,175	13,859	251
	214	9,342,840	60,602	43,658	283
	513	5,042,040	4,423	9,829	8.62
Average				**26,286**	**642**
s.d.				10,493	663
Ttest p=				**0.003**	**0.98**

Table S2d: siRNA inhibition of PrP endocytosis at 90 minutes

siRNA	Con		LRP1.1		LRP1.2		LRP1.3	
Endocytosis	**PrP**	**Tf**	**PrP**	**Tf**	**PrP**	**Tf**	**PrP**	**Tf**
Cells analsysed	76.8%	87.3%	47.1%	63.7%	80.6%	85.0%	66.6%	59.2%
	75.2%	88.4%	51.7%	76.9%	52.9%	82.4%	77.6%	98.9%
	75.2%	86.0%	52.8%	82.3%	80.2%	90.7%	55.6%	83.4%
	76.8%	87.3%	42.0%	94.7%	78.3%	84.8%	74.8%	81.7%
	75.2%	88.9%	26.8%	82.9%	66.3%	91.7%	66.8%	77.3%
	67.5%	86.0%	34.0%	90.6%	80.9%	69.5%	76.2%	81.8%
	98.2%	58.6%	28.3%	44.9%	23.6%	79.4%	71.1%	82.4%
	59.1%	89.2%	39.8%	92.0%	35.9%	81.8%	88.2%	86.8%
	37.7%	92.1%	54.2%	67.2%	79.6%	93.4%	88.9%	67.0%
	90.3%	88.1%	52.9%	97.2%	66.6%	95.1%	81.6%	98.0%
	95.1%	96.2%	66.0%	92.7%	78.2%	91.5%	73.0%	61.2%
	96.7%	93.4%	45.1%	80.5%	39.4%	84.6%	33.6%	96.8%
	80.3%	79.8%	78.1%	87.5%	56.3%	88.2%	81.0%	73.4%
	98.2%	87.6%	56.5%	84.8%	44.6%	71.6%	87.1%	93.7%
	100.0%	96.1%	47.5%	69.5%	75.0%	88.7%	59.9%	76.5%
	91.7%	93.0%	30.5%	80.1%	77.3%	83.5%	47.2%	91.8%
	95.9%	94.9%			67.8%	87.9%	55.0%	88.4%
	86.4%	93.3%			80.5%	74.8%	48.6%	89.8%
	51.6%	94.8%			37.0%	89.5%		
	97.9%	91.4%			37.3%	91.1%		
	76.7%	80.7%			85.7%	84.5%		
	85.4%	91.3%						
	73.2%	97.1%						
	89.7%	97.1%						
	98.6%	97.9%						
	88.2%	82.7%						
	87.3%	87.8%						
PrP^C vs PrP^C, siRNA con vs LRP1, unpaired T test, p =	96.3%	96.7%						
	92.9%	93.3%						
	81.2%	73.5%	0.0000000005		**0.0001**		**0.001**	
	98.3%	77.7%						
	99.0%	92.2%						
PrP vs Tf endocytosed by each cell, paired T test, p =	78.1%	80.7%						
	99.1%	98.1%						
	89.4%	80.6%	**0.0000007**		**0.00006**		**0.01**	
	59.6%	46.6%						
	99.8%	73.8%						
	99.5%	99.5%						
	91.1%	94.7%						
Average	**84.9%**	**87.5%**	**47.1%**	**80.5%**	**63.0%**	**85.2%**	**68.5%**	**82.7%**
s.d.	15.0%	10.9%	14.2%	13.7%	26.0%	7.1%	26.3%	11.9%

Table S3a: Sustained inhibition of LRP1 lowers surface PrP^C

Expt Ref:	siRNA	Mean PrP surface Fluorescence Intensity	± s.d.	No. cells analysed	% of control, p value **
6/12/05	Control	2,028,535	538,086	12	
	LRP1.1	739,787	83,824	10	36.5%***
24/1/06	Control	15,561,640	2,653,561	17	
	LRP1.1	5,918,709	1,901,410	11	38.0%***
25/11/05	Control	4,553,347	2,757,167	7	
	LRP1.1	2,449,245	1,103,537	9	53.8%**
24/2/06	Control	4,209,806	868,900	5	
	LRP1.1	1,990,312	402,111	7	47.3%**
				Average	**43.9%**
				s.d.	8.1%

Table S3b. Sustained inhibition of LRP1 increases surface Thy-1

Cell	Thy-1 Fluor intensity	Volume µm3	Relative Intensity	% of control
C-1	31,610,300	1,271	24,870	
C-1a	42,398,900	1,488	28,494	
C-2	10,215,800	1,698	6,016	
C-3	6,780,090	614	11,042	
C-4	9,196,590	1,202	7,651	
C-3a	37,303,200	962	38,777	
C-6	27,751,000	2,626	10,568	
C6a	10,634,500	1,967	5,406	
Average	**21,986,298**	**1,479**	**16,603**	
s.d.	14,339,498	625	12,458	
siRNA-1	61,976,600	2,058	30,115	
siRNA-2	58,280,800	1,566	37,216	
siRNA-3	34,432,600	543	63,412	
siRNA-4	24,757,700	1,898	13,044	
siRNA-1	61,976,600	2,058	30,115	
siRNA-2	58,280,800	1,566	37,216	
siRNA-3	34,432,600	543	63,412	
siRNA-4	24,757,700	1,898	13,044	
Average	**44,861,925**	**1,516**	**35,947**	**216.5%**
s.d.	16,783,742	630	19,380	
Ttest			**0.04**	

Table S4a: Sustained inhibition (4hours) of LRP1 increases the total cellular PrP and BiP, but not significantly, αMannosidase II and Syntaxin 6 (Table 3 and Fig. 4)

	Vol cell	Fluorescence Intensity normalized for volume sampled		Vol cell	Fluorescence Intensity normalized for volume sampled		Vol cell	Fluorescence Intensity normalized for volume sampled	
	µm3	**BiP**	**PrP**	**µm3**	**αMann II**	**PrP**	**µm3**	**Syntaxin 6**	**PrP**
siRNAcontrol treated cells	516	597,349	329,047	1,258	248,899	131,827	1,323	1,557,099	369,985
	1,585	1,143,441	1,218,559	751	3,435,769	1,128,165	621	6,075,057	835,496
	1,553	1,937,662	4,476,710	2,042	169,014	245,807	925	3,315,030	857,184
	662	472,785	15,114,559	2,944	477,323	383,128	535	2,889,960	498,329
	788	469,914	3,270,172	554	4,021,753	629,020	2,180	1,046,594	224,511
	1,363	229,706	7,305,440	1,178	2,175,062	688,612			
	1,327	279,020	1,774,218	2,124	2,191,014	409,179			
	2,885	6,654,756	82,105	1,190	4,239,758	1,232,694			
	1,674	5,686,521	24,383	1,019	2,498,608	343,755			
	817	4,657,809	406,976	879	9,948,033	995,504			
	1,722	1,162,555	390,953	1,349	1,294,353	197,280			
				413	4,631,214	294,706			
				360	4,115,870	440,700			
				837	65,594	2,411,151			
				2,031	39,749	1,571,199			
				888	69,148	1,886,376			
Mean	**1,354**	**2,117,411**	**3,126,647**	**1,239**	**2,476,323**	**811,819**	**962**	**2,976,748**	**557,101**
S.D.		2,373,712	4,583,514		2,620,057	672,273		1,966,112	281,352
siRNA-LRP1.1 treated cells	1,502	267,972	6,954,028	1,234	2,700,245	2,087,068			
	1,590	1,672,205	10,965,064	415	8,692,160	2,613,120			
	881	6,240,086	4,093,975	763	1,357,634	612,130			
	1,098	487,941	16,973,420	1,669	1,246,570	746,324			
	1,129	3,353,731	1,964,998	770	3,617,606	4,117,994			
	2,250	15,686,523	9,069,159	818	6,570,927	3,546,431			
	1,300	14,117,658	13,513,271	772	5,489,297	4,424,700			
	912	14,587,540	3,231,581	2,631	2,270,262	943,883	624	4,229,084	969,771
	2,256	28,402,927	10,204,587	565	4,639,667	1,378,540	907	6,356,861	465,116
	1,552	16,287,034	1,151,059	757	7,517,824	3,609,137	875	2,560,980	1,775,540
	620	908,525	6,016,930	804	3,166,896	8,197,139	884	3,336,634	857,237
				775	712,616	9,919,996	1,521	3,383,012	5,575,019
				1,350	375,343	3,712,004			
				886	341,525	3,142,118			
Mean	**1,372**	**9,273,831**	**7,648,916**	1,015	**3,478,469**	**3,503,613**	**1,117**	**3,973,314**	**1,928,537**
s.d.		9,155,543	5,007,077		2,734,888	2,695,340		1,457,328	2,093,368
as % control		**438%**	**245%**		**140%**	**432%**		**133%**	**346%**
Ttest, p =		**0.028**	**0.039**		**0.316**	**0.003**		**0.391**	**0.218**

Table S4b: overlap of PrP with biosynthetic comparment markers (for Table 3 & Fig. 6)

	PrP Fluorescence intensity	BiP fluorescence intensity	PrP overlapping with BiP	BiP overlapping with PrP	% PrP overlapping with BiP	% BiP overlapping with PrP
*con1	9,522,890	6,109,370	3,828,840	3,708,630	40.2%	60.7%
*con2	13,392,700	10,022,900	3,522,760	2,216,320	26.3%	22.1%
*con3	5,962,630	6,582,040	2,950,420	2,518,450	49.5%	38.3%
*con4	18,846,900	8,479,870	8,114,620	6,998,390	43.1%	82.5%
con3	10,212,700	8,855,410	3,863,360	4,565,290	37.8%	51.6%
con01	2,062,560	1,474,410	603,697	954,756	29.3%	64.8%
con4	4,732,940	2,544,200	860,865	756,920	18.2%	29.8%
con 02	1,205,040	1,812,370	604,026	1,576,670	50.1%	87.0%
Mean	**4,553,310**	**3,671,598**	**1,482,987**	**1,963,409**	**36.8%**	**54.6%**
s.d.	4,061,022	3,484,599	1,591,533	1,769,402	10.6%	22.1%
*siRNA-3	6,061,610	2,706,250	1,135,240	626,847	18.7%	23.2%
*siRNA-5	19,526,500	18,782,300	12,242,300	7,661,830	62.7%	40.8%
*siRNA-6	8,218,600	6,857,260	3,037,720	2,050,460	37.0%	29.9%
*siRNA-10	7,364,690	4,178,470	3,807,400	2,693,570	51.7%	64.5%
siRNA-01a	5,157,380	4,669,290	984,832	581,776	19.1%	12.5%
siRNA-01b	4,275,600	3,642,040	984,832	581,776	23.0%	16.0%
siRNA-07	2,505,530	3,189,300	464,706	350,706	18.5%	11.0%
siRNA-08	7,433,380	6,488,140	1,149,400	2,707,490	15.5%	41.7%
Mean	**4,842,973**	**4,497,193**	**895,943**	**1,055,437**	**30.8%**	**29.9%**
s.d.	2,048,952	1,464,623	297,774	1,106,742	17.8%	18.3%
Ttest					0.435	0.036
Cell	**PrP**	**aMannII**	**PrP on Mann**	**Mann on PrP**	**%PrP/Mann**	**%Mann/PrP**
C3	2,510,250	2,910,150	774,562	1,493,440	30.9%	51.3%
C4	1,175,230	6,750,870	345,141	1,299,890	29.4%	19.3%
C5	1,242,650	9,186,890	216,070	1,406,950	17.4%	15.3%
C7	1,943,620	2,232,070	132,549	347,275	6.8%	15.6%
C8	632,514	2,696,430	128,995	471,690	20.4%	17.5%
C10	3,237,390	4,022,490	547,882	1,485,310	16.9%	36.9%
C11	1,254,680	1,736,190	338,130	595,491	26.9%	34.3%
C12	1,587,710	2,206,750	250,894	685,711	15.8%	31.1%
C13	2,531,170	4,107,800	404,911	1,028,700	16.0%	25.0%
C14	5,016,300	9,897,430	614,195	1,952,210	12.2%	19.7%
C15	1,535,780	4,197,920	543,646	1,594,720	35.4%	38.0%
C16	3,024,700	8,372,510	1,104,760	2,982,990	36.5%	35.6%
Average	**2,141,000**	**4,859,792**	**450,145**	**1,278,698**	**22.1%**	**28.3%**
s.d.	1,207,971	2,921,756	286,529	736,300	9.5%	11.3%
LRP 4	3,215,280	4,088,290	552,031	1,424,570	17.2%	34.8%
LRP 5	4,827,390	7,855,930	1,467,600	4,399,460	30.4%	56.0%
LRP 7	4,250,250	4,889,920	1,140,140	2,559,090	26.8%	52.3%
LRP 8	1,827,980	3,049,060	396,592	1,222,870	21.7%	40.1%
LRP 9	5,833,400	8,879,010	1,613,280	4,723,000	27.7%	53.2%
LRP 10	2,148,070	10,847,100	304,041	890,584	14.2%	8.2%
LRP 11	2,870,110	8,583,570	470,189	1,324,470	16.4%	15.4%
LRP 12	4,513,410	11,748,700	1,077,930	3,617,600	23.9%	30.8%
LRP 13	4,254,360	15,044,800	1,585,070	7,984,610	37.3%	53.1%
LRP 14	1,882,600	7,547,360	536,506	1,585,350	28.5%	21.0%
LRP 15	2,430,050	4,343,690	442,282	1,732,540	18.2%	39.9%
LRP 16	1,035,520	1,970,040	183,514	540,114	17.7%	27.4%
Average	**3,257,368**	**7,403,956**	**814,098**	**2,667,022**	**23.3%**	**36.0%**
s.d.	1,464,577	3,908,946	528,327	2,165,322	7.0%	16.0%

	PrP	Syntaxin 6	PrP on Syn6	Syn6 on PrP	%PrP/Syn6	%Syn6/PrP
control-02	969,771	4,229,084	412,110	337,422	42.5	8.0
control-02a	465,116	6,356,861	192,019	1,167,566	41.3	18.4
control-03	1,775,540	2,560,980	154,931	615,382	8.7	24.0
control0-01	857,237	3,336,634	123,118	343,032	14.4	10.3
control-05	5,575,019	3,383,012	1,138,542	1,557,562	20.4	46.0
Mean	**1,928,537**	**3,973,314**	**404,144**	**804,193**	**25.5**	**21.3**
s.d.	550,065	1,639,070	130,777	390,018	17.7	7.4
siRNA-01	3,063,184	1,557,099	369,985	708,364	12.1	45.5
siRNA-02	2,820,595	6,075,057	835,496	1,308,767	29.6	21.5
siRNA-04	3,207,594	3,315,030	857,184	1,313,991	26.7	39.6
siRNA-05	2,714,860	2,889,960	498,329	471,176	18.4	16.3
siRNA-06	1,214,249	420,369	70,482	161,373	5.8	38.4
siRNA-06a	2,059,793	1,046,594	224,511	268,044	10.9	25.6
Mean	**2,154,325**	**2,186,301**	**407,998**	**604,531**	**18.3**	**28.3**
s.d.	750,024	2,044,910	320,615	505,282	10.7	11.8
Ttest					0.34	0.27

Table S5a: Heat shock does not change the level of surface PrP on neurons

Surface PrP immunofluorescence intensity per µm3 of cell sampled	37˚C	39˚C
	1,828	399
	3,012	1,911
	1,938	1,660
	8,322	627
	856	1,875
	851	4,583
	567	1,152
Average	**2,482**	**1,744**
s.d.	2,711	1,386
T test, p =	**0.54**	

Table S5b: Heat shock (4 hours, 39˚C) elevates intracellular BiP, but not PrP[c]

Cell	Fluorescence Intensity BiP	Fluorescence Intensity PrP	Volume (µm3)	BIP/µm3	PRP/µm3
37.1	594,373	2,611,780	380	1,564	6,873
37.3	1,380,990	335,247	109	12,670	3,076
37.4	223,177	16,770	137	1,629	122
37.5	5,065,700	1,242,560	134	37,804	9,273
37.6	809,928	464,251	399	2,030	1,164
37.7	1,104,070	344,151	74	14,920	4,651
37.8	545,192	234,558	123	4,432	1,907
37.9	10,096,000	1,882,970	1,050	9,615	1,793
37.10	541,373	1,943,440	299	1,811	6,500
			Average	**9,608**	**3,929**
			s.d.	10,614	3,602
39.2	1,691,820	473,142	72	23,498	6,571
39.3	5,418,540	555,865	110	49,259	5,053
39.4	2,457,740	514,186	156	15,755	3,296
39.5	4,673,460	1,016,360	195	23,966	5,212
39.7	732,015	383,590	150	4,880	2,557
39.8	7,561,750	660,854	263	28,752	2,513
39.9	4,256,710	704,134	461	9,234	1,527
39.10	3,368,390	469,594	500	6,737	939
39.11	5,524,900	73,163	174	31,752	420
39.16	16,917,700	15,069	358	47,256	42
39.17	10,941,200	244,828	375	29,177	653
39.12	11,785,200	733,124	301	39,153	2,436
39.13	2,827,190	263,171	163	17,345	1,615
39.14	3,333,170	889,336	164	20,324	5,423
39.15	1,198,480	705,998	86	13,936	8,209
			Average	**24,068**	**3,098**
			s.d	13,698	2,461
			Ratio 39/37C	**2.50**	**0.79**
			T TEST, p =	**0.015**	**0.47**

Table S6a: *Surface PrPc on Tg20 is 14X higher than WT, LRP1 is 1.8 fold*

	Cell	Fluorescence Intensity LRP	Fluorescence Intensity PrP	Volume (μm3)	LRP/μm3	PrP/μm3	Ratio LRP:PrP
Wild type neurons	1a.1	9,325,250	795,165	764	12,206	1,041	11.7
	1a.2	5,693,950	56,501	966	5,894	58	100.8
	1a.3	7,171,900	1,733,030	958	7,486	1,809	4.1
	1a.4	972,051	85,938	520	1,869	165	11.3
	1a.5	7,590,390	779,754	1,214	6,252	642	9.7
	1a.6	6,058,320	405,207	832	7,282	487	15.0
	1a.7	14,873,600	320,728	1,540	9,658	208	46.4
	1a.8	1,044,400	144,171	491	2,127	294	7.2
	1a.9	8,505,650	1,272,730	800	10,632	1,591	6.7
	1a.10	3,763,280	423,214	829	4,540	511	8.9
	1a.11	1,099,870	138,381	478	2,301	290	7.9
	1a.12	2,049,490	431,445	321	6,385	1,344	4.8
	Aver	**5,679,013**	**548,855**	**809**	**6,386**	**703**	**9.1**
	s.d.	4,191,969	516,233	341	3,351	596	28
Tg20 neurons	1b.1	3,365,390	750,557	477	7,055	1,573	4.5
	1b.2	5,100,470	1,693,040	292	17,467	5,798	3.0
	1b.3	4,519,710	3,950,010	452	9,999	8,739	1.1
	1b.4	4,785,770	5,627,890	388	12,334	14,505	0.9
	1b.5	1,839,850	6,583,510	581	3,167	11,331	0.3
	1b.6	2,852,730	10,629,500	498	5,728	21,344	0.3
	1b.7	5,340,770	10,877,800	485	11,012	22,428	0.5
	1b.8	5,794,700	6,430,920	531	10,913	12,111	0.9
	1b.9	4,422,530	4,359,150	610	7,250	7,146	1.0
	1b.10	6,461,740	1,412,520	556	11,622	2,541	4.6
	1b.11	11,647,800	2,872,200	525	22,186	5,471	4.1
	1b.12	4,884,410	1,446,600	247	19,775	5,857	3.4
	Aver	**5,084,656**	**4,719,475**	**470**	**11,542**	**9,904**	**1.2**
	s.d.	2,428,886	3,448,002	111	5,740	6,751	2
			T test, Tg20 vs Wild Type, P =		**0.015**	**0.0006**	**0.05**
			Ratio Tg20:Wild Type, =		**1.8**	**14.1**	**1:8**

Table 6b: BiP levels on normal compared to Tg20 sensory neurons

	WT	**Tg20**
BiP fluorescence intensity for individual cells	3,694,360	23,781,800
	8,187,440	5,664,300
	13,826,500	7,639,520
	5,554,800	8,901,670
	7,320,500	7,037,240
Average	**7,716,720**	**10,604,906**
s.d.	3,826,266	7,457,595
T Test, p =	**0.470**	